

Towards Practical Large-scale Randomized Iterative Least Squares Solvers through Uncertainty Quantification *

Nathaniel Pritchard[†] and Vivak Patel[‡]

Abstract. As the scale of problems and data used for experimental design, signal processing and data assimilation grows, the oft-occurring least squares subproblems are correspondingly growing in size. As the scale of these least squares problems creates prohibitive memory movement costs for the usual incremental QR and Krylov-based algorithms, randomized least squares problems are garnering more attention. However, these randomized least squares solvers are difficult to integrate application algorithms as their uncertainty limits practical tracking of algorithmic progress and reliable stopping. Accordingly, in this work, we develop theoretically-rigorous, practical tools for quantifying the uncertainty of an important class of iterative randomized least squares algorithms, which we then use to track algorithmic progress and create a stopping condition. We demonstrate the effectiveness of our algorithm by solving a 0.78 TB least squares subproblem from the inner loop of incremental 4D-Var using only 195 MB of memory.

Key words. random sketching, linear systems, iterative methods, residual estimation, stopping criterion, least-squares, Coordinate Descent

AMS subject classifications. 65F10, 65F25, 60F10, 62L12

1. Introduction. Least squares problems are regularly solved as core subproblems in a variety of important algorithms for experimental design [13, 3], signal processing [23, 25], data assimilation [26, 8], and uncertainty quantification [27, 24]. Moreover, these least squares subproblems are growing in both the number of equations and the dimension of the unknown variables owing to two pressures: (1) improvements in technology have increased the permeation of higher-frequency sensors, which grows the volume of data being used and which, in turn, (usually) increases the number of equations in the least squares subproblem; and (2) the growing desire for more accurately simulating models (e.g., using finer meshes for partial differential equation models) increases the number of unknown variables in the least squares problems.

Unfortunately, the growth of least squares subproblems is a challenge for commonly used solvers. For instance, solving a least squares problem with many observations can be addressed in a memory-efficient manner using an incremental QR algorithm [16], so long as the resulting upper triangular term can be fit in memory. Unfortunately, if the number of unknowns is sufficiently larger, this least squares incremental QR algorithm will be unable to store and manipulate the resulting upper triangular matrix without substantial slowdowns induced by memory movement costs. As another example, Krylov-based least squares solvers can also be efficiently deployed [9], so long as matrix-vector and matrix-transpose-vector products can be efficiently computed. Unfortunately, if the system is sufficiently large that it cannot be stored in memory, then Krylov-based least squares solvers are substantially slowed down also because

* Authors are supported by UW-Madison WARF Award AAD5914.

[†]Department of Statistics, University of Wisconsin - Madison (npritchard@wisc.edu).

[‡]Department of Statistics, University of Wisconsin - Madison (vivak.patel@wisc.edu, vivakpatel.org).

of the memory movement costs needed to read in the matrix multiple times per iteration [14].

As these challenges to standard solvers are driven by size, randomized least squares solvers (e.g., iterative Hessian sketch [21] and generalized column subspace descent [19, 18, 20]) seem to be promising alternatives as they are able to compress the information in the original linear system to more manageable dimensions. However, such iterative randomized least squares solvers must first overcome a key practical challenge: as such solvers would be called repeatedly within an iterative algorithm, their solution accuracy must be controlled so as to ensure the efficiency of the algorithm. For example, in incremental 4D-Var [4], a least squares subproblem occurs at every iteration of the algorithm. Indeed, in the initial few iterations, the least squares subproblem need only be solved to low accuracy as this is usually enough to generate progress quickly, while later iterations will demand that the subproblem be solved to higher accuracy. Thus, achieving such control over the least square subproblem solver's accuracy ensures the efficiency of the overall algorithm.

When it comes to solving least squares problems, controlling the solver's accuracy depends on tracking the progress of the iterations and defining clear stopping conditions, which are typically achieved by using the norm of the gradient of the least squares subproblem. Unfortunately, the gradient of a large least squares problem is calculated by applying a very large matrix in both its original and transposed orientation to a vector—a procedure that is very costly because of its guaranteed violation of the principal of spatial locality for memory accesses [14] (excepting the case in which the matrix is symmetric). This issue is further exacerbated for a randomized solver: the gradient at the iterates of a randomized solver *is never explicitly calculated*, and, even if it were calculated occasionally for monitoring progress, it would be less reliable as we now explain. As the iterates of the randomized solver are random, the gradient evaluated at these iterates inherits this randomness; thus, a wide range of gradient norm values would correspond to the same absolute error in the iterates (see the blue boxes in Figure 1), which results in the norm of the gradient being a poor reflection of the absolute error. To reiterate, the gradient norm is widely used for tracking and stopping least squares problems, but it is infeasible to calculate for large scale problems, and is unreliable for randomized solvers.

In the class of sketching-based randomized solvers that we consider in this work, the infeasibility of calculating the entire gradient can be addressed by using the sketch of the gradient, which *is efficiently and regularly calculated by this class of randomized solvers*.¹ However, the sketched gradient norm inherits not only the randomness of the gradient at an iterate, but also the randomness from the sketching procedure. To see this, as shown by the red boxes in Figure 1, the sketched gradient norm has an even wider range for the same absolute error relative to the gradient norm. Thus, the sketched gradient norm, though feasibly calculated, is even less reliable for tracking and stopping an iterative randomized least squares solver.

While the sketched gradient norm alone is insufficient to reliably track and stop the un-

¹While there are cases where this is not true, we generally accept the premise that randomly sketching a matrix can be efficiently calculated. For instance, the Fast Johnson-Lindenstrauss Transform leverages the fast fourier transform to efficiently sketch a matrix [2]. As another example, a Gaussian sketch can be efficiently applied using emerging photonic hardware, e.g., lighton.ai.

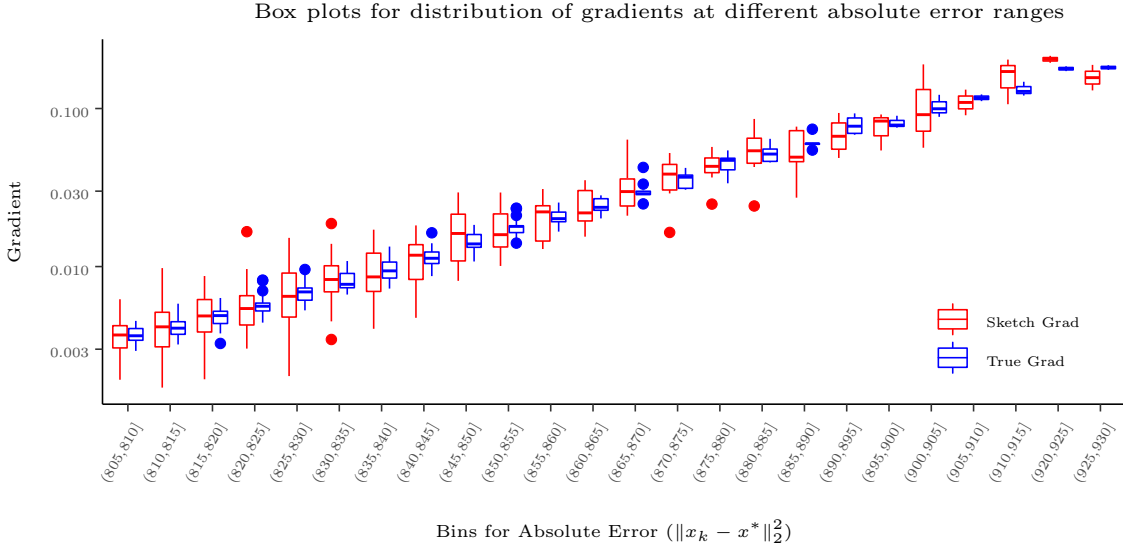


Figure 1. We solve a *randsvd* linear system from *MatrixDepot* [29] using an iterative random sketching method, the norm squared of the true and sketched gradients of the iterates as well as the absolute error of the iterates is calculated. The plot shows box plots of the distribution of gradient values for the norms of the sketched and true gradients, for different bins of absolute error.

derlying randomized least squares solver, if the sketched gradient norm’s uncertainty could be quantified, then we could use this uncertainty set to create risk-informed² metrics for tracking and stopping the corresponding underlying algorithm. In this work, we develop a practical, computationally-efficient method for quantifying the uncertainty set of the sketched gradient, and use it to develop risk-informed methods for tracking and stopping the underlying algorithm. In fact, we take this a step further by generalizing our method to a moving average of the sketched gradient, which turns out to be more reliable. We emphasize that our method requires only a small additional computational and memory cost over the solver, will accurately reflect the algorithm’s progress based on a user-defined threshold for risk, and will stop the algorithm based on a user-defined threshold for risk. We demonstrate the power of our methodology by solving a 0.78 TB least squares subproblem arising from the incremental 4D-Var algorithm using only 195 MB of memory, for which LSQR is infeasible (see [subsection 5.4](#)). As a result of our methodology, we are enabling the practical integration of an important class of randomized least squares solvers into algorithms that are widely used in science and engineering, which will support solving larger problems in these fields.

The remainder of this paper is organized as follows. In [section 2](#), we tabulate important notation. In [section 3](#), we specify the problem that we are solving, the algorithm used to solve this problem, our moving average of the norm of the gradient estimator, our estimate of its uncertainty set, and our stopping condition. In [section 4](#), we rigorously establish the foundations of our estimators. In [section 5](#), we numerically demonstrate the effectiveness

²By risk-informed, we mean that the user can specify probabilities for which the tracking metrics and stopping conditions can fail.

of our estimators and compare our algorithm to a state-of-the-art solver. In [section 6](#), we conclude.

2. Notation. We use the following the notation in this work.

Symbol	Description
A	A coefficient matrix in $\mathbb{R}^{m \times n}$.
B	A symmetric positive definite matrix in $\mathbb{R}^{m \times m}$.
b	A constant vector in \mathbb{R}^m .
S_k	A random matrix in $\mathbb{R}^{m \times p}$ that satisfies the Johnson-Lindenstrauss property (See Definition 3.1).
$\ \cdot\ _2$	The standard Euclidean norm.
x_k	The iterate at iteration k .
r_k	The residual at iteration k , i.e., $r_k = Ax_k - b$.
g_k	The gradient of the least squares problem at iteration k , i.e., $g_k = A'Br_k$.
\tilde{g}_k	The sketched gradient of the least squares problem at iteration k , i.e., $S'_{k+1}g_k$.
\mathcal{P}	The orthogonal projection matrix onto the range of $B^{1/2}A$.
ρ_k^λ	The moving average with window width λ of the norms squared of the gradients of the least squares problem.
ι_k^λ	The moving average with window width λ of the norms to the fourth power of the gradients of the least squares problem.
$\tilde{\rho}_k^\lambda$	The moving average with window width λ of the norms squared of the sketched gradients of the least squares problem.
$\tilde{\iota}_k^\lambda$	The moving average with window width λ of the norms to the fourth power of the sketched gradients of the least squares problem.
$\mathbf{SE}(\sigma^2, \omega)$	A sub-Exponential distribution with variance bounded by σ^2 and scale parameter ω .
d	Reserved for moments of a distribution.
η	User defined constriction parameter used in the calculations of interval width and stopping condition.
Q_k	A matrix with orthonormal columns.
τ_ℓ	Stopping times.
ξ_I	User specified control on probability of stopping too late.
ξ_{II}	User specified control on probability of stopping too early.

v	User specified threshold for a small enough ρ_k^λ to warrant stopping.
$\mathbb{E}[\cdot]$	The expectation operator.
$\mathbb{P}(\cdot)$	The probability measure.
\mathcal{F}_k	The σ -algebra generated by S_1, \dots, S_k

3. Problem Formulation & Algorithm. We are interested in solving the following minimization problem

$$(3.1) \quad \min_{x \in \mathbb{R}^n} \|Ax - b\|_B^2,$$

where $A \in \mathbb{R}^{m \times n}$ is a coefficient matrix; $B \in \mathbb{R}^{m \times m}$ is any symmetric positive definite matrix; $b \in \mathbb{R}^m$ is a constant vector; and both m and n are large. Note, we allow m and n to be arbitrary, so our methodology applies to overdetermined, underdetermined, and rank-deficient systems. Owing to the size of A , we can only access A through matrix-vector multiplications; similarly, *though we will not need it in our algorithm*, we can access A^\top through matrix-vector multiplications, though this would be substantially more expensive owing to the needed memory access pattern [14]. For all other operations, we make use of efficiently-computed (see [Footnote 1](#)), sketches of A , which we individually denote by (possibly with a subscript)

$$(3.2) \quad \tilde{A} = AS \in \mathbb{R}^{m \times p},$$

where p is generally significantly smaller than n (see [Remark 4.6](#)); and $S \in \mathbb{R}^{n \times p}$ is a random matrix that satisfies the Johnson–Lindenstrauss property [11] defined in the following manner.

Definition 3.1. A matrix $S \in \mathbb{R}^{n \times p}$ satisfies the Johnson–Lindenstrauss property if there exists constants $C, \omega > 0$ such that for all $\delta \geq 0$ and for any $x \in \mathbb{R}^n$,

$$(3.3) \quad \mathbb{P}(|\|Sx\|_2^2 - \|x\|_2^2| > \delta \|x\|_2^2) < 2e^{-\min\{Cp\delta^2, (Cp\delta)/\omega\}}.$$

Remark 3.2. In [Definition 3.1](#), the constants C and ω are determined by the method used to generate S . There are many choices of these methods, such as sparse Rademacher matrices [1], Fast Johnson Lindenstrauss Transform (FJLT) [2], and Gaussian matrices [5, 10, 15]. For these examples, the values of C and ω are supplied in [Table 2](#).

Remark 3.3. By [Definition 3.1](#), $\|Sx\|_2^2$ is a sub-exponential random variable with parameters $(1/(Cp), \omega)$ [28].

To solve this problem we will employ an important subclass of generalized column-space descent methods (see [20]), which begins with an iterate $x_0 \in \mathbb{R}^n$ and generates a sequence of iterates, $\{x_k : k \in \mathbb{N}\}$, according to the recursive equation

$$(3.4) \quad x_k = x_{k-1} - S_k(\tilde{A}_k^\top B \tilde{A}_k)^\dagger \tilde{A}_k^\top B(Ax_{k-1} - b),$$

where \dagger is the Moore-Penrose pseudoinverse; $\{S_k : k \in \mathbb{N}\}$ are independent, identically distributed matrices satisfying [Definition 3.1](#); and $\tilde{A}_k = AS_k$, which can be computed efficiently (see [Footnote 1](#)). The update [\(3.4\)](#) is mathematically equivalent to the update,

$$(3.5) \quad x_k = x_{k-1} - S_k(S_k^\top A^\top B A S_k)^\dagger S_k^\top A^\top B(Ax_{k-1} - b),$$

which is a form that will be useful for proving theory relating to the convergence of [\(3.4\)](#), but which **we do not explicitly use for the algorithm as A^\top is unfavorable to access for large matrices**.

Under this formulation, [Algorithm 3.1](#) presents our methodology for practically tracking and stopping the progress of least squares solvers of the form [\(3.5\)](#) for matrices $\{S_k\}$ that satisfy [Definition 3.1](#). [Algorithm 3.1](#) has several key components that we explain presently.

1. At each iteration, we compute estimators of two key quantities to determine the progress and uncertainty of the algorithm. One quantity we wish to estimate is the moving average of the norms squared of the gradients, ρ_k^λ , which we define as

$$(3.6) \quad \rho_k^\lambda = \sum_{i=k-\lambda+1}^k \frac{\|g_i\|_2^2}{\lambda},$$

where $g_k = A_k^\top B(Ax_k - b)$ is the gradient at iterate x_k ; and where λ is the width of the moving window. When $\lambda = 1$, we recover just the gradient at iteration x_k , and, when $\lambda > 1$, we have a moving average of the gradients. As it is infeasible to calculate ρ_k^λ , we estimate ρ_k^λ with the sketched gradients *that have already been computed in the updates of our algorithm* (see [\(3.4\)](#)),

$$(3.7) \quad \tilde{\rho}_k^\lambda = \sum_{i=k-\lambda+1}^k \frac{\|\tilde{g}_i\|_2^2}{\lambda},$$

where $\tilde{g}_k = A_k^\top B(Ax_k - b)$. When $\lambda = 1$, we recover the sketched gradient norm at iterate x_k , and, when $\lambda > 1$, we have a moving average of the sketched gradient norms, which turns out to be more reliable.

2. As discussed in [section 1](#), we need to quantify the uncertainty in $\tilde{\rho}_k^\lambda$ in order to develop risk-informed (i.e., where the user defines probabilities for failure) tracking metrics and stopping conditions. To estimate this uncertainty, we estimate an upper bound on the

Table 2
Values of C and ω in [Definition 3.1](#) for common sampling methods.

	C	ω
Gaussian Matrix [5]	0.23467	.1127
Achlioptas [1]	0.23467	.1127
FJLT [2]	0.03125	.0625

variance of $\rho_k^\lambda - \tilde{\rho}_k^\lambda$. As will be seen in [subsection 4.3](#), this variance upper bound has two multiplicative parts, one that is constant and one that varies across iterations. The portion of this variance upper bound that varies across iterations is estimated using the moving average of the norms to the fourth power of the gradients,

$$(3.8) \quad \iota_k^\lambda = \sum_{i=k-\lambda+1}^k \frac{\|g_i\|_2^4}{\lambda}.$$

Similar to ρ_k^λ , computation of ι_k^λ is impractical. Hence, we estimate ι_k^λ using

$$(3.9) \quad \tilde{\iota}_k^\lambda = \sum_{i=k-\lambda+1}^k \frac{\|\tilde{g}_i\|_2^4}{\lambda}.$$

3. The matrix $B^{1/2}$ is square root of the positive definite matrix, $B \in \mathbb{R}^{m \times m}$, used in the general norm. In practice, $B^{1/2}$ can be computed using the Cholesky decomposition, if B is not too dense or large. Fortunately, in many problems that we consider, such as 4D-Var, B has an underlying structure that can be exploited to efficiently compute $B^{1/2}$.

4. The constants C, ω , and p play an important role in the algorithm due to their relationship with [Definition 3.1](#). The parameters C and ω are constants relating to the size of the tail bound described in [Definition 3.1](#). Their values, which depend on the chosen sampling method, can be found in [Table 2](#). The constant p is the embedding dimension of the random matrix S_k , and also appears in the tail bound of [Definition 3.1](#). A small lower bound on the size of p is necessary for convergence (see [Lemma 4.5](#), [Remark 4.6](#)).

5. Line 2 contains the conditions for stopping the algorithm. If ρ_k^λ could be practically calculated, then the algorithm could be stopped when ρ_k^λ falls below a user-specified threshold, v . However, since we must instead use the estimator of ρ_k^λ , $\tilde{\rho}_k^\lambda$. Stopping when $\tilde{\rho}_k^\lambda \leq v$ leads to two possible sources of error.

5a. One type of error is associated with stopping the algorithm later than desired. Algorithmically, this scenario arises when $\rho_k^\lambda \leq v$ while $\tilde{\rho}_k^\lambda > v$. To control this error, we need two user-specified quantities. The first quantity specifies how far ρ_k^λ is below v . In particular, we let the user choose $\delta_I \in (0, 1)$, and we control the probability that $\rho_k^\lambda \leq \delta_I v$ while $\tilde{\rho}_k^\lambda > v$. The second quantity is a user specified bound on this probability, ξ_I , that indicates the user's level of risk tolerance for possibly stopping too late.

5b. The second type of error is associated with stopping too early. Algorithmically, this scenario occurs when $\rho_k^\lambda > v$, while $\tilde{\rho}_k^\lambda \leq v$. Similarly to the first scenario, we will let the user choose $\delta_{II} > 1$ to quantify how much larger ρ_k^λ is in comparison to v , when $\tilde{\rho}_k^\lambda < v$. Then, we control this probability with a user-specified value ξ_{II} , which reflects the user's level of risk tolerance for potentially stopping too early.

6. The user-specified parameter η is an optional parameter to adjust for the conservativeness of the theoretical confidence interval and stopping condition. If the user specifies $\eta = 1$, then there is no adjustment. Reasonable, yet still conservative choices for η can be found in [Table 3](#), which are based on numerical simulations.

7. Lines 7 through 11 adaptively change the window width of the moving average. This procedure is necessary as there are two distinct phases of convergence in the algorithm. In the

first phase, the iterates converge rapidly towards the solution, which necessitates a smaller moving average window width to reduce the impact of earlier iterates. In the second phase, the iterates begin to make less progress and the randomness of the algorithm is more pronounced in their behavior, which necessitates a larger moving average window width to smooth out this randomness. We identify the change point between the two phases to be the iteration where the norm of the sketched gradients are no longer monotonically decreasing, i.e., $\|\tilde{g}_k\|_2^2 > \|\tilde{g}_{k-1}\|_2^2$. At this point we slowly increase the width of the window from the narrow window width, λ_1 , by one at each iteration until it reaches that of the wide window width, λ_2 . While we choose the monotonic condition because of its simplicity and effectiveness, other conditions that attempt to estimate the change point between phases could also be used.

8. Lines 12 and 13 inexpensively update the estimators $\tilde{\rho}_k^\lambda$ and $\tilde{\iota}_k^\lambda$, requiring only four floating point operations to calculate. However, this update can suffer from issues of numerical stability, especially for $\tilde{\iota}_k^\lambda$. If this is a concern, then $\tilde{\rho}_k^\lambda$ and $\tilde{\iota}_k^\lambda$ can be computed in $\mathcal{O}(\lambda_2)$ time simply by taking the mean of the nonzero entries in its storage vector, ρ or ι .

9. Line 16 describes a $1 - \alpha$ credible interval designed to contain ρ_k^λ using the estimators $\tilde{\rho}_k^\lambda$ and $\tilde{\iota}_k^\lambda$ computed at iteration k . As with the stopping condition, this credible interval is derived in [subsection 4.3](#) from the tail bounding distribution described in [subsection 4.2](#). The parameter α is selected by the user.

Table 3
Table of Conservative η values for three sampling methods

Method	η
Gaussian	4
FJLT	24
Achlioptas	4

4. Validity of the Credible Interval and Stopping Condition. With an understanding of the parts of [Algorithm 3.1](#), we must now demonstrate the validity of [Algorithm 3.1](#). In particular, we must show that Line 16 is a valid credible interval for ρ_k^λ , and we must show that Line 2 controls the probabilities of the two aforementioned errors at ξ_I and ξ_{II} . As both the credible interval and stopping condition depend on $\tilde{\rho}_k^\lambda$ and $\tilde{\iota}_k^\lambda$, we will need to establish the validity of these two estimators (i.e., their consistency) in order to establish the validity of the credible interval and stopping condition. In turn, as the consistency of $\tilde{\rho}_k^\lambda$ and $\tilde{\iota}_k^\lambda$ depends on the convergence of the iterates, $\{x_k\}$, we show the convergence of the iterates in [subsection 4.1](#) (specifically, see [Theorem 4.7](#)). Then, we show that $\tilde{\rho}_k^\lambda$ and $\tilde{\iota}_k^\lambda$ are consistent estimators for their respective quantities ρ_k^λ and ι_k^λ by deriving a tail bound for both quantities (see [subsection 4.2](#) and [Theorems 4.8 and 4.9](#)). Now that we have established the validity of $\tilde{\rho}_k^\lambda$ and $\tilde{\iota}_k^\lambda$, we derive the credible interval (see [subsection 4.2](#) and [Corollary 4.10](#)) and stopping condition (see [subsection 4.2](#) and [Corollary 4.11](#)). Both the credible interval and stopping condition require a quantity that is impractical to compute, so we establish that using $\tilde{\iota}_k^\lambda$ as a plug-in estimator for the impractical quantity controls the relative error between the theoretical values for the credible interval and stopping condition, and the versions that use the plug-in estimator (see [subsection 4.3](#) and [Lemma 4.12](#)).

Algorithm 3.1 Tracking and Stopping for Least Squares

Require: $A \in \mathbb{R}^{m \times n}$, $b \in \mathbb{R}^m$, $B^{1/2} \in \mathbb{R}^{m \times m}$, $x_0 \in \mathbb{R}^n$.

Require: $\{S_k\}$ satisfying [Definition 3.1](#).

Require: Moving average window widths $\lambda_1 \leq \lambda_2 \in \mathbb{N}$.

Require: $\alpha > 0$, $\xi_I \in (0, 1)$, $\xi_{II} \in (0, 1)$, $\delta_I \in (0, 1)$, $\delta_{II} > 1$, $\eta \geq 1$, $v > 0$.

1: $k \leftarrow 0$, $k' \leftarrow \infty$, $\tilde{\rho}_0^* \leftarrow 0$, $\tilde{\iota}_0^* \leftarrow 0$, $\lambda_o \leftarrow 0$, $\lambda \leftarrow \lambda_1$, $\rho \leftarrow \{0\}^{\lambda_2}$, $\iota \leftarrow \{0\}^{\lambda_2}$

2: **while** $k == 0$ **or** $\tilde{\rho}_k^\lambda \geq v$ **or**

$$\begin{aligned} \tilde{\iota}_k^\lambda \geq \min \left\{ \frac{Cp\lambda\eta \min\{(1 - \delta_I)^2 v^2, (1 - \delta_I)v/\omega\}}{(1 + \log(\lambda)) \log(2/\xi_I)}, \right. \\ \left. \frac{Cp\lambda\eta \min\{(\delta_{II} - 1)^2 v^2, (\delta_{II} - 1)v/\omega\}}{(1 + \log(\lambda)) \log(2/\xi_{II})} \right\} \end{aligned}$$

do

3: # Iteration k #

4: $r_k \leftarrow B^{1/2}(Ax_k - b)$

5: $\tilde{A}_{k+1} \leftarrow B^{1/2}AS_{k+1}$

6: $\tilde{g}_{k+1} \leftarrow \tilde{A}_{k+1}^\top r_k$

7: **if** $\|\tilde{g}_{k+1}\|_2^2 \geq \|\tilde{g}_k\|_2^2$ **then**

8: $k' \leftarrow k + 1$

9: **end if**

10: $\lambda_o \leftarrow \lambda$

11: $\lambda \leftarrow \begin{cases} \min(k + 1, \lambda_1) & k + 1 \leq k' \text{ or } k' = \infty \\ \min(\lambda_1 + 1 + (k + 1 - k'), \lambda_2) & k + 1 > k' \end{cases}$

12: $\tilde{\rho}_{k+1}^\lambda \leftarrow \frac{\lambda_o \tilde{\rho}_k^\lambda + \|\tilde{g}_{k+1}\|_2^2 - \rho[(k+1) \bmod \lambda_2]}{\lambda}$

13: $\tilde{\iota}_{k+1}^\lambda \leftarrow \frac{\lambda_o \tilde{\iota}_k^\lambda + \|\tilde{g}_{k+1}\|_2^2 - \iota[(k+1) \bmod \lambda_2]}{\lambda}$

14: $\rho[(k + 1) \bmod \lambda_2] \leftarrow \|\tilde{g}_{k+1}\|_2^2$

15: $\iota[(k + 1) \bmod \lambda_2] \leftarrow \|\tilde{g}_{k+1}\|_2^4$

16: Update the estimated $(1 - \alpha)$ -interval by computing:

$$\tilde{\rho}_{k+1}^\lambda \pm \max \left(\sqrt{\frac{2 \log(2/\alpha) \tilde{\iota}_{k+1}^\lambda (1 + \log(\lambda))}{Cp\lambda\eta}}, \frac{2 \log(2/\alpha) \tilde{\iota}_{k+1}^\lambda (1 + \log(\lambda)) \omega}{Cp\lambda\eta} \right)$$

17: $u_{k+1} \leftarrow \operatorname{argmin}_u \|\tilde{A}_{k+1}u - r_k\|_2^2$ # See [16] and [9]

18: $x_{k+1} \leftarrow x_k - S_k u_{k+1}$

19: $k \leftarrow k + 1$

20: **end while**

21: **return** x_k and estimated $(1 - \alpha)$ -interval

4.1. Convergence of the Iterates. To show that the iterates converge to a solution, it is equivalent to show that the gradient of the least squares problem goes to zero. In turn, if B is the identity matrix, it is equivalent to show that the component of the residual of the linear system in the column space of A goes to zero. For general B , an analogous equivalence is established in the following lemma.

Lemma 4.1. *Let $A \in \mathbb{R}^{m \times n}$, $B \in \mathbb{R}^{m \times m}$ be positive definite, and $x \in \mathbb{R}^n$. Let \mathcal{P} be the orthogonal projection onto $\text{col}(B^{1/2}A)$. Then, the gradient of the least squares problem at x , $A^\top B(Ax - b) = 0$ if and only if $\mathcal{P}B^{1/2}(Ax - b) = 0$.*

Proof. Let $r = Ax - b$. Suppose $A^\top Br = 0$,

$$(4.1) \quad 0 = A^\top Br = A^\top B^{1/2}(\mathcal{P}B^{1/2}r + (I - \mathcal{P})B^{1/2}r) = A^\top B^{1/2}\mathcal{P}B^{1/2}r,$$

Where the last equality comes from $I - \mathcal{P}$ being an orthogonal projector onto the null space of $A^\top B^{1/2}$. Since, $\mathcal{P}B^{1/2}r$ is in the range of $B^{1/2}A$ we know that $A^\top B^{1/2}\mathcal{P}B^{1/2}r$ will only be zero when $\mathcal{P}B^{1/2}r = 0$.

Now suppose $\mathcal{P}B^{1/2}r = 0$. Then,

$$(4.2) \quad A^\top Br = A^\top B^{1/2}(\mathcal{P}B^{1/2}r + (I - \mathcal{P})B^{1/2}r) = A^\top B^{1/2}(I - \mathcal{P})B^{1/2}r = 0,$$

where the last equality follows from $I - \mathcal{P}$ being an orthogonal projector onto the null space of $A^\top B^{1/2}$. ■

As the preceding lemma establishes, showing $\{\mathcal{P}B^{1/2}r_k\} \rightarrow 0$ is equivalent to showing that the iterates converge to a solution. Thus, we establish a recursive relationship between $\mathcal{P}B^{1/2}r_{k+1}$ and $\mathcal{P}B^{1/2}r_k$. From (3.5),

$$(4.3) \quad r_k = (I - AS_k(S_k^\top A^\top BAS_k)^\dagger S_k^\top A^\top B)r_{k-1}.$$

Multiplying both sides by $B^{1/2}$,

$$(4.4) \quad B^{1/2}r_k = (I - B^{1/2}AS_k(S_k^\top A^\top BAS_k)^\dagger S_k^\top A^\top B^{1/2})B^{1/2}r_{k-1}.$$

From here, let $\psi_k = B^{1/2}r_k$. Since $\text{col}(B^{1/2}A) \supset \text{col}(B^{1/2}AS_k)$, multiplying both sides by \mathcal{P} produces

$$(4.5) \quad \mathcal{P}\psi_k = (I - B^{1/2}AS_k(S_k^\top A^\top BAS_k)^\dagger S_k^\top A^\top B^{1/2})\mathcal{P}\psi_{k-1}.$$

Finally, since $B^{1/2}AS_k(S_k^\top A^\top BAS_k)^\dagger S_k^\top A^\top B^{1/2}$ is an orthogonal projection matrix, we can define a matrix Q_k to be the matrix with orthonormal columns that span $\text{col}(B^{1/2}AS_k)$. Then we can write (4.5) as

$$(4.6) \quad \mathcal{P}\psi_k = (I - Q_k Q_k^\top) \mathcal{P}\psi_{k-1}.$$

With these relationships and notations established, we now turn to establishing convergence.

Geometric Reduction in Residual Components that lie in Column space of $B^{1/2}A$. Let $\tau_0 = 0$ and τ_1 being the first iteration where

$$(4.7) \quad \text{col}(Q_1) + \text{col}(Q_2) + \cdots + \text{col}(Q_{\tau_1}) = \text{col}(B^{1/2}A),$$

is satisfied. Noting that if (4.7) is not satisfied then τ_1 is infinite; otherwise, τ_1 is finite and the following lemma holds.

Lemma 4.2. *Let $\psi_0 \in \mathbb{R}^m$ and let $\{\mathcal{P}\psi_k\}$ be generated according to (4.5) for $\{S_k : k \in \mathbb{N}\}$, which are independent and identically distributed random matrices satisfying Definition 3.1. On the event, $\{\tau_1 < \infty\}$ there exists a $\gamma_1 \in (0, 1)$ such that*

$$(4.8) \quad \|\mathcal{P}\psi_{\tau_1}\|_2 \leq \gamma_1 \|\mathcal{P}\psi_0\|_2.$$

Proof. To prove this, it is only necessary to show that γ_1 exists. First, let $q_{k,1}, \dots, q_{k,p}$ denote the columns of Q_k . Then we can write ψ_{τ_1} by (4.6) as,

$$(4.9) \quad \mathcal{P}\psi_{\tau_1} = \left[\prod_{k=1}^{\tau_1} \left(I - q_{k,j} q_{k,j}^\top \right) \right] \mathcal{P}\psi_0.$$

Since $\mathcal{P}\psi_0 \in \text{col}(B^{1/2}A)$, [19, Theorem 4.1] implies that there $\exists \gamma_1 \in (0, 1)$ that is a function of $\{q_{1,1}, q_{1,2}, \dots, q_{\tau_1,p}\}$ such that $\|\mathcal{P}\psi_{\tau_1}\|_2 \leq \gamma_1 \|\mathcal{P}\psi_0\|_2$. \blacksquare

We can easily repeat this argument for more than just τ_1 , in fact when $\{\tau_\ell < \infty\}$, define $\tau_{\ell+1}$ to be the first iteration after τ_ℓ where,

$$(4.10) \quad \text{col}(Q_{\tau_\ell+1}) + \text{col}(Q_{\tau_\ell+2}) + \cdots + \text{col}(Q_{\tau_{\ell+1}}) = \text{col}(B^{1/2}A),$$

otherwise let $\tau_{\ell+1}$ be infinite. The preceding argument for the existence of $\gamma_1 \in (0, 1)$ will then result in the following corollary.

Corollary 4.3. *Let $\psi_0 \in \mathbb{R}^m$ and let $\{\mathcal{P}\psi_k\}$ be generated according to (4.5) for $\{S_k : k \in \mathbb{N}\}$, which are independent and identically distributed random matrices satisfying Definition 3.1. On the event, $\cap_{\ell=1}^L \{\tau_\ell < \infty\}$ there exist $\gamma_\ell \in (0, 1)$ for $\ell = 1, \dots, L$, such that*

$$(4.11) \quad \|\mathcal{P}\psi_{\tau_L}\|_2 \leq \left(\prod_{\ell=1}^L \gamma_\ell \right) \|\mathcal{P}\psi_0\|_2.$$

Control of Random Rate and Random Iteration. While appearing to indicate the convergence of the $\mathcal{P}\psi_k$, Corollary 4.3 does not guarantee that the portion of the ψ_k in the range of $B^{1/2}A$ converges to 0. This lack of guarantee for convergence arises from two possible points of failure, one being the case where $\gamma_\ell \rightarrow 1$ as $\ell \rightarrow \infty$ and the other being the case where τ_ℓ is infinite. The following result addresses the former issue using the independence of $\{S_k\}$.

Lemma 4.4. *Let $\{S_k : k \in \mathbb{N}\}$ be independent and identically distributed random variables. If for any $\ell \in \mathbb{N}$, $\tau_{\ell-1}$ is finite, then $\{\tau_j - \tau_{j-1} : j \leq \ell\}$ exist and are independent and identically distributed; and $\{\gamma_j : j \leq \ell\}$ are independent and identically distributed.*

Proof. When τ_ℓ is finite, [7, Theorem 4.1.3] states that $\{Q_{\tau_\ell+1}, \dots, Q_{\tau_\ell+k}\}$ given τ_ℓ are independent of $\{Q_1, \dots, Q_{\tau_\ell}\}$ and are identically distributed to $\{Q_1, \dots, Q_k\}$ for all k . Therefore, $\tau_{\ell+1} - \tau_\ell$ and τ_1 are independent and identically distributed. It follows that γ_ℓ are independent and identically distributed. \blacksquare

So far, we only know that $\tau_0 = 0$ is finite. Hence, we only know that the random variable $\tau_1 - \tau_0$ exists, but we do not know anything about its finiteness. The next result provides the appropriate remedy.

Lemma 4.5. *Let $\{S_k : k \in \mathbb{N}\}$ be independent and identically distributed random variables satisfying Definition 3.1. If*

$$(4.12) \quad p > \frac{\log(2)}{C} \max \left\{ \omega^2, \frac{1}{\delta^2} \right\},$$

for some $\delta \in (0, 1)$, then $\exists \pi \in (0, 1]$ such that for all $\ell \in \mathbb{N}$ and $k \geq \text{rank}(A)$,

$$(4.13) \quad \mathbb{P}(\tau_\ell - \tau_{\ell-1} = k) \leq \binom{k-1}{\text{rank}(A)-1} (1-\pi)^{k-\text{rank}(A)} \pi^{\text{rank}(A)}.$$

Proof. We begin by verifying that for $z \in \text{col}(B^{1/2}A)$ and $z \neq 0$, then $S^\top A^\top B^{1/2}z \neq 0$ with some nonzero probability. Definition 3.1 implies that for any $\delta \in (0, 1)$,

$$(4.14) \quad \mathbb{P}(\|S^\top A^\top B^{1/2}z\|_2^2 > 0) \geq \mathbb{P} \left(\left| \|S^\top A^\top B^{1/2}z\|_2^2 - \|A^\top B^{1/2}z\|_2^2 \right| \leq \delta \|A^\top B^{1/2}z\|_2^2 \right) \\ (4.15) \quad \geq 1 - 2e^{-\min\{Cp\delta^2, Cp\delta/\omega\}}.$$

When $\delta \in (0, 1)$ is chosen such that (4.12) holds, then $1 - 2e^{-\min\{Cp\delta^2, Cp\delta/\omega\}} > 0$. Moreover, as this bound is independent of $z \in \text{col}(B^{1/2}A)$, we will refer to the lower bound of $\mathbb{P}(\|S^\top A^\top B^{1/2}z\|_2^2 > 0)$ by $\pi \in (0, 1]$ for any $z \neq 0$. Thus, due to the relationship between Q_k and $\text{col}(B^{1/2}AS_k)$, $\mathbb{P}(\|Q_k^\top z\|_2 > 0) \geq \pi$ for all $z \neq 0$.

Given that $\{\text{col}(Q_k) : k \in \mathbb{N}\}$ are independent and identically distributed, we conclude that the probability that $\text{col}(Q_1) + \dots + \text{col}(Q_{k+1})$ increases in dimension from $\text{col}(Q_1) + \dots + \text{col}(Q_k)$, when $\dim(\text{col}(Q_1) + \dots + \text{col}(Q_{k+1})) < \text{rank}(A)$ is at least π . This implies that the probability that the dimension increases $\text{rank}(A)$ times in the first k iterations with $k > \text{rank}(A)$ is dominated by a negative binomial distribution, i.e., for $k \geq \text{rank}(A)$,

$$(4.16) \quad \mathbb{P}(\tau_1 = k) \leq \binom{k-1}{\text{rank}(A)-1} (1-\pi)^{k-\text{rank}(A)} \pi^{\text{rank}(A)}.$$

As a result, τ_1 is finite with probability one. The result follows by Lemma 4.4. \blacksquare

Remark 4.6. If $\delta = 1$, for the Gaussian and Achlioptas sampling methods one should choose $p > 2$ to ensure convergence, while for FJLT sampling method one should choose $p > 22$ to satisfy the hypothesis of Lemma 4.5.

Convergence of the Moments. With the establishment of the previous lemmas we can now conclude the following theorem.

Theorem 4.7. *Let $x_0 \in \mathbb{R}^n$ and let \mathcal{P} be the orthogonal projection onto $\text{col}(B^{1/2}A)$. Suppose that $\{S_k : k \in \mathbb{N}\}$ are independent and identically distributed random variables satisfying Definition 3.1 and (4.12) for some $\delta \in (0, 1)$. Let $\{x_k : k \in \mathbb{N}\}$ be generated according to (3.4). Define $\psi_k = B^{1/2}(Ax_k - b)$. Then for any $d \in \mathbb{N}$, $\mathbb{E}[\|\mathcal{P}\psi_k\|_2^d] \rightarrow 0$ and $\mathbb{E}[\|g_k\|_2^d] = \mathbb{E}[\|A^\top B(Ax_k - b)\|_2^d] \rightarrow 0$ as $k \rightarrow \infty$. Furthermore, for any particular ℓ we have*

$$(4.17) \quad \mathbb{E}[\|\mathcal{P}\psi_{\tau_\ell}\|_2^d] \leq \mathbb{E}[\gamma_1^d]^\ell \|\mathcal{P}\psi_0\|_2^d.$$

Proof. It is enough to show that $\mathbb{E}[\|\mathcal{P}\psi_{\tau_\ell}\|_2^d] \rightarrow 0$ as $k \rightarrow \infty$. By Lemma 4.2, $\|\mathcal{P}\psi_k\|_2$ is a non-increasing sequence. Thus, we only need to show a subsequence converges to zero. By Corollary 4.3 and Lemma 4.4 and Lemma 4.5,

$$(4.18) \quad \mathbb{E}[\|\mathcal{P}\psi_{\tau_\ell}\|_2^d] \leq \mathbb{E}[\gamma_1^d]^\ell \|\mathcal{P}\psi_0\|_2^d,$$

for all $\ell \in \mathbb{N}$, where $\mathbb{E}[\gamma_1^d] < 1$. Therefore, as $\ell \rightarrow \infty$, the conclusion follows. \blacksquare

4.2. Theoretical Values for the Credible Interval and Stopping Condition. With convergence in all moments established, we now turn to understanding the distributions of $\tilde{\rho}_k^\lambda$ and $\tilde{\iota}_k^\lambda$, in order to validate the estimators as well as derive the stopping condition and credible interval. We begin with an examination of the distribution of $\tilde{\rho}_k^\lambda$. Intuitively, if the terms were independent, we would trivially have that $\tilde{\rho}_k^\lambda$ satisfies Definition 3.1, as the terms in the definition of $\tilde{\rho}_k^\lambda$ satisfy the Definition 3.1. Unfortunately, *they are not independent*. Thus, we innovate the following method to derive the distribution of $\tilde{\rho}_k^\lambda$ to handle the dependencies, which results in only an additional logarithmic term relative to what would have been the case if the terms had been independent.

Theorem 4.8. *Suppose the setting of Theorem 4.7. Define $\mathcal{F}_{k-\lambda+1}$ be the σ -algebra generated by $S_1, \dots, S_{k-\lambda+1}$, then*

$$(4.19) \quad \tilde{\rho}_k^\lambda - \rho_k^\lambda \Big| \mathcal{F}_{k-\lambda+1} \sim \text{SE} \left(\frac{M_{k-\lambda+1}^4 (1 + \log(\lambda))}{2Cp\lambda}, \omega \right),$$

where $M_{k-\lambda+1} = \|A^\top B^{1/2}\|_2 \|\mathcal{P}B^{1/2}r_{k-\lambda+1}\|_2$ and $r_{k-\lambda+1} = Ax_{k-\lambda+1} - b$.

Proof. By induction, we prove, for $|t| \leq 1/\omega$,

$$(4.20) \quad \mathbb{E} \left[\prod_{i=k-\lambda+1}^k \exp \left\{ \frac{t}{\lambda} (\|\tilde{g}_i\|_2^2 - \|g_i\|_2^2) \right\} \right] \Big| \mathcal{F}_{k-\lambda+1} \leq \exp \left(\frac{t^2 M_{k-\lambda+1}^4}{2Cp\lambda} \sum_{j=1}^\lambda \frac{1}{j} \right),$$

where $M_{k-\lambda+1} = \|A^\top B^{1/2}\|_2 \|\mathcal{P}B^{1/2}r_{k-\lambda+1}\|_2$. We can then use a logarithm to bound the summation. As a result, the sub-exponential distribution of $\tilde{\rho}_k^\lambda - \rho_k^\lambda$ follows by [22, Lemma A.4].

The base case of $\lambda = 1$ follows trivially from $\|\tilde{g}_{k-\lambda+1}\|_2^2$ being sub-Exponential. Now assume that the result holds for $k - \lambda + 1$ to $k - 1$. Then,

$$(4.21) \quad \mathbb{E} \left[\prod_{i=k-\lambda+1}^k \exp \left\{ \frac{t}{\lambda} (\|\tilde{g}_i\|_2^2 - \|g_i\|_2^2) \right\} \middle| \mathcal{F}_{k-\lambda+1} \right]$$

$$(4.22) \quad = \mathbb{E} \left[\mathbb{E} \left[\prod_{i=k-\lambda+1}^k \exp \left\{ \frac{t}{\lambda} (\|\tilde{g}_i\|_2^2 - \|g_i\|_2^2) \right\} \middle| \mathcal{F}_k \right] \middle| \mathcal{F}_{k-\lambda+1} \right]$$

$$= \mathbb{E} \left[\mathbb{E} \left[\exp \left\{ \frac{t}{\lambda} (\|\tilde{g}_k\|_2^2 - \|g_k\|_2^2) \right\} \middle| \mathcal{F}_k \right] \right]$$

$$(4.23) \quad \times \prod_{i=k-\lambda+1}^{k-1} \exp \left\{ \frac{t}{\lambda} (\|\tilde{g}_i\|_2^2 - \|g_i\|_2^2) \right\} \middle| \mathcal{F}_{k-\lambda+1}$$

$$(4.24) \quad \leq \mathbb{E} \left[\exp \left\{ \frac{t^2 \|g_k\|_2^4}{2\lambda^2 Cp} \right\} \prod_{i=k-\lambda+1}^{k-1} \exp \left\{ \frac{t}{\lambda} (\|\tilde{g}_i\|_2^2 - \|g_i\|_2^2) \right\} \middle| \mathcal{F}_{k-\lambda+1} \right],$$

where we have made use of $\|\tilde{g}_k\|_2^2$ being sub-Exponential in the ultimate line. Now, applying Hölder's inequality and the induction hypothesis,

$$(4.25) \quad \mathbb{E} \left[\exp \left\{ \frac{t^2 \|g_k\|_2^4}{2\lambda^2 Cp} \right\} \prod_{i=k-\lambda+1}^{k-1} \exp \left\{ \frac{t}{\lambda} (\|\tilde{g}_i\|_2^2 - \|g_i\|_2^2) \right\} \middle| \mathcal{F}_{k-\lambda+1} \right]$$

$$\leq \mathbb{E} \left[\exp \left\{ \frac{t^2 \|g_k\|_2^4}{2\lambda Cp} \right\} \middle| \mathcal{F}_{k-\lambda+1} \right]^{\frac{1}{\lambda}}$$

$$(4.26) \quad \times \mathbb{E} \left[\prod_{i=k-\lambda+1}^{k-1} \exp \left\{ \frac{t}{\lambda-1} (\|\tilde{g}_i\|_2^2 - \|g_i\|_2^2) \right\} \middle| \mathcal{F}_{k-\lambda+1} \right]^{\frac{\lambda-1}{\lambda}}$$

$$(4.27) \quad \leq \mathbb{E} \left[\exp \left\{ \frac{t^2 \|g_k\|_2^4}{2\lambda Cp} \right\} \middle| \mathcal{F}_{k-\lambda+1} \right]^{\frac{1}{\lambda}} \exp \left\{ \frac{t^2 M_{k-\lambda+1}^4}{2Cp(\lambda-1)} \sum_{j=1}^{\lambda-1} \frac{1}{j} \right\}^{\frac{\lambda-1}{\lambda}}.$$

Now, [Lemmas 4.1](#) and [4.4](#) and [Corollary 4.3](#) imply, with probability one,

$$(4.28) \quad \|g_k\|_2^4 \leq \|A^\top B^{1/2}\|_2^4 \|\mathcal{P}B^{1/2}r_k\|_2^4 \leq \|A^\top B^{1/2}\|_2^4 \|\mathcal{P}B^{1/2}r_{k-\lambda+1}\|_2^4 = M_{k-\lambda+1}^4.$$

Since $M_{k-\lambda+1}$ is measurable with respect to $\mathcal{F}_{k-\lambda+1}$, we apply the inequality of (4.28) to (4.27) to conclude the proof by induction. \blacksquare

With the establishment of the distribution around the difference between $\tilde{\rho}_k^\lambda$ and ρ_k^λ , we also obtain the consistency of $\tilde{\rho}_k^\lambda$ for ρ_k^λ from [Theorem 4.8](#) by allowing $k \rightarrow \infty$, using the Sub-Exponential tail bound [28, Proposition 2.9], and using the dominated convergence theorem to switch the limit and the integral. With this consistency result, **we conclude that $\tilde{\rho}_k^\lambda$ is a valid estimator for ρ_k^λ** .

We now turn to showing the validity of $\tilde{\iota}_k^\lambda$ as an estimator. To show the validity of $\tilde{\iota}_k^\lambda$ we transform $\tilde{\iota}_k^\lambda - \iota_k^\lambda$ into a form where we can make repeated applications of (4.20). After making these applications, we get the consistency result for $\tilde{\iota}_k^\lambda$ presented in the following theorem.

Theorem 4.9. *Under the conditions of Theorem 4.7, we have*

$$(4.29) \quad \mathbb{P} \left(\left| \tilde{\iota}_k^\lambda - \iota_k^\lambda \right| > \epsilon \middle| \mathcal{F}_{k-\lambda+1} \right) \leq (1 + \lambda) \exp \left(- \frac{\epsilon^2 C p \lambda}{2 \left(2 M_{k-\lambda+1}^2 + \left(\frac{\epsilon^2 \lambda}{(1 + \log(\lambda))} \right)^{1/4} \right)^2 M_{k-\lambda+1}^4 (1 + \log(\lambda))} \right),$$

where $M_{k-\lambda+1} = \|A^\top B^{1/2}\|_2 \|\mathcal{P}B^{1/2}r_{k-\lambda+1}\|_2$ and $r_{k-\lambda+1} = Ax_{k-\lambda+1} - b$. Thus, as $k \rightarrow \infty$, $\tilde{\iota}_k^\lambda$ is a consistent estimator for ι_k^λ .

Proof. Using the definitions of ι_k^λ and $\tilde{\iota}_k^\lambda$ we have

$$(4.30) \quad \mathbb{P} \left(\left| \tilde{\iota}_k^\lambda - \iota_k^\lambda \right| > \epsilon \middle| \mathcal{F}_{k-\lambda+1} \right)$$

$$(4.31) \quad = \mathbb{P} \left(\left| \sum_{i=k-\lambda+1}^k \frac{\|\tilde{g}_i\|_2^4 - \|g_i\|_2^4}{\lambda} \right| > \epsilon \middle| \mathcal{F}_{k-\lambda+1} \right)$$

$$(4.32) \quad \leq \mathbb{P} \left(\sum_{i=k-\lambda+1}^k \left| \frac{\|\tilde{g}_i\|_2^4 - \|g_i\|_2^4}{\lambda} \right| > \epsilon \middle| \mathcal{F}_{k-\lambda+1} \right)$$

$$(4.33) \quad \leq \mathbb{P} \left(\sum_{i=k-\lambda+1}^k \left| \frac{\|\tilde{g}_i\|_2^2 - \|g_i\|_2^2}{\lambda} \right| \left| \|\tilde{g}_i\|_2^2 + \|g_i\|_2^2 \right| > \epsilon \middle| \mathcal{F}_{k-\lambda+1} \right).$$

Then, using any constant $G > 2M_{k-\lambda+1}^2$, we partition (4.33) into disjoint sets. Thus,

$$(4.34) \quad \mathbb{P} \left(\sum_{i=k-\lambda+1}^k \left| \frac{\|\tilde{g}_i\|_2^2 - \|g_i\|_2^2}{\lambda} \right| \left| \|\tilde{g}_i\|_2^2 + \|g_i\|_2^2 \right| > \epsilon \middle| \mathcal{F}_{k-\lambda+1} \right)$$

$$(4.35) \quad = \mathbb{P} \left(\sum_{i=k-\lambda+1}^k \left| \frac{\|\tilde{g}_i\|_2^2 - \|g_i\|_2^2}{\lambda} \right| \left| \|\tilde{g}_i\|_2^2 + \|g_i\|_2^2 \right| > \epsilon, \right.$$

$$\left. \bigcap_{i=k-\lambda+1}^k \left\{ \left| \|\tilde{g}_i\|_2^2 + \|g_i\|_2^2 \right| \leq G \right\} \middle| \mathcal{F}_{k-\lambda+1} \right)$$

$$+ \mathbb{P} \left(\sum_{i=k-\lambda+1}^k \left| \frac{\|\tilde{g}_i\|_2^2 - \|g_i\|_2^2}{\lambda} \right| \left| \|\tilde{g}_i\|_2^2 + \|g_i\|_2^2 \right| > \epsilon, \right.$$

$$\left. \bigcup_{i=k-\lambda+1}^k \left\{ \left| \|\tilde{g}_i\|_2^2 + \|g_i\|_2^2 \right| > G \right\} \middle| \mathcal{F}_{k-\lambda+1} \right)$$

$$(4.36) \quad \begin{aligned} &\leq \mathbb{P} \left(\sum_{i=k-\lambda+1}^k \left| \frac{\|\tilde{g}_i\|_2^2 - \|g_i\|_2^2}{\lambda} \right| > \frac{\epsilon}{G} \middle| \mathcal{F}_{k-\lambda+1} \right) \\ &\quad + \mathbb{P} \left(\bigcup_{i=k-\lambda+1}^k \{|\|\tilde{g}_i\|_2^2 + \|g_i\|_2^2| > G\} \middle| \mathcal{F}_{k-\lambda+1} \right). \end{aligned}$$

From here, we present the bounds for the top and bottom terms of (4.36) separately. For the top term of (4.36) we use (4.20) to get,

$$(4.37) \quad \mathbb{P} \left(\sum_{i=k-\lambda+1}^k \left| \frac{\|\tilde{g}_i\|_2^2 - \|g_i\|_2^2}{\lambda} \right| > \frac{\epsilon}{G} \middle| \mathcal{F}_{k-\lambda+1} \right) \leq \exp \left(\frac{t^2 M_{k-\lambda+1}^4 (1 + \log(\lambda))}{2Cp\lambda} - \frac{\epsilon t}{G} \right)$$

$$(4.38) \quad \leq \exp \left(-\frac{\epsilon^2 Cp\lambda}{2G^2 M_{k-\lambda+1}^4 (1 + \log(\lambda))} \right),$$

where (4.38) comes from minimizing (4.37) in terms of t . We next address the bottom of (4.36) for which we have

$$(4.39) \quad \mathbb{P} \left(\bigcup_{i=k-\lambda+1}^k \{|\|\tilde{g}_i\|_2^2 + \|g_i\|_2^2| > G\} \middle| \mathcal{F}_{k-\lambda+1} \right)$$

$$(4.40) \quad = \mathbb{P} \left(\bigcup_{i=k-\lambda+1}^k \{|\|\tilde{g}_i\|_2^2 - \|g_i\|_2^2 + 2\|g_i\|_2^2| > G\} \middle| \mathcal{F}_{k-\lambda+1} \right)$$

$$(4.41) \quad \leq \mathbb{P} \left(\bigcup_{i=k-\lambda+1}^k \{|\|\tilde{g}_i\|_2^2 - \|g_i\|_2^2 + 2M_{k-\lambda+1}^2| > G\} \middle| \mathcal{F}_{k-\lambda+1} \right)$$

$$(4.42) \quad \leq \sum_{i=k-\lambda+1}^k \mathbb{P} \left(|\|\tilde{g}_i\|_2^2 - \|g_i\|_2^2| > G - 2M_{k-\lambda+1}^2 \middle| \mathcal{F}_{k-\lambda+1} \right)$$

$$(4.43) \quad \leq \lambda \exp \left(\frac{t^2 M_{k-\lambda+1}^4}{2Cp} - t (G - 2M_{k-\lambda+1}^2) \right)$$

$$(4.44) \quad \leq \lambda \exp \left(-\frac{Cp (G - 2M_{k-\lambda+1}^2)^2}{2M_{k-\lambda+1}^4} \right),$$

where (4.41) comes from (4.28), (4.43) comes from the (4.20), and (4.44) comes from minimizing (4.43) in terms of t . Putting both parts together gives us (4.29).

From (4.29), we begin the proof of consistency by first observing that when $G \geq 2M_{k-\lambda+1}^2 + \left(\frac{\epsilon^2 \lambda}{(1 + \log(\lambda))} \right)^{1/4} > 2M_{k-\lambda+1}^2$ it is the case that

$$(4.45) \quad \exp \left(-\frac{\epsilon^2 Cp\lambda}{2G^2 M_{k-\lambda+1}^4 (1 + \log(\lambda))} \right) \geq \exp \left(-\frac{Cp (G - 2M_{k-\lambda+1}^2)^2}{2M_{k-\lambda+1}^4} \right).$$

Thus, if we let $Y = 2M_{k-\lambda+1}^2 + \left(\frac{\epsilon^2\lambda}{(1+\log(\lambda))}\right)^{1/4}$ we can upper bound the right-hand side of (4.29) in the following manner,

$$(4.46) \quad \inf_{G>2M_{k-\lambda+1}^2} \exp\left(-\frac{\epsilon^2 Cp\lambda}{2G^2 M_{k-\lambda+1}^4 (1+\log(\lambda))}\right) + \lambda \exp\left(-\frac{Cp(G-2M_{k-\lambda+1}^2)^2}{2M_{k-\lambda+1}^4}\right)$$

$$(4.47) \quad \leq \inf_{G>Y} (1+\lambda) \exp\left(-\frac{\epsilon^2 Cp\lambda}{2G^2 M_{k-\lambda+1}^4 (1+\log(\lambda))}\right)$$

$$(4.48) \quad \leq (1+\lambda) \exp\left(-\frac{\epsilon^2 Cp\lambda}{2\left(2M_{k-\lambda+1}^2 + \left(\frac{\epsilon^2\lambda}{(1+\log(\lambda))}\right)^{1/4}\right)^2 M_{k-\lambda+1}^4 (1+\log(\lambda))}\right),$$

where the last line comes from recognizing that (4.47) is monotonically increasing when $G > 0$. We then conclude consistency by recognizing that Theorem 4.7 implies that $M_{k-\lambda+1} \rightarrow 0$ as $k \rightarrow \infty$ and then applying the dominated convergence theorem to switch the limit and the integral. \blacksquare

With the consistency and distributional results now established, we conclude that our estimators are valid; thus, we are now able to derive the credible interval corresponding to Line 16 and the stopping condition corresponding to Line 2 of Algorithm 3.1.

Corollary 4.10. *Under the conditions of Theorem 4.7, a credible interval of level $1 - \alpha$ for $\tilde{\rho}_k^\lambda$, corresponding to Line 16 in Algorithm 3.1, is*

$$(4.49) \quad \tilde{\rho}_k^\lambda \pm \max\left(\sqrt{2\log(2/\alpha)\frac{M_{k-\lambda+1}^4(1+\log(\lambda))}{Cp\lambda}}, 2\log(2/\alpha)\frac{M_{k-\lambda+1}^4(1+\log(\lambda))\omega}{Cp\lambda}\right).$$

Proof. Using the sub-Exponential variance from Theorem 4.8 and the tail bound result from [28, Proposition 2.9],

$$(4.50) \quad \mathbb{P}\left(\left|\tilde{\rho}_k^\lambda - \rho_k^\lambda\right| > \epsilon | \mathcal{F}_{k-\lambda+1}\right) \leq 2 \exp\left(-\frac{Cp\lambda}{2M_{k-\lambda+1}^4(1+\log(\lambda))} \min\left(\epsilon^2, \frac{\epsilon}{\omega}\right)\right).$$

From this tail probability it should be clear that the high probability region is controlled by the choice of ϵ ; thus, if we choose ϵ to correspond to a specific quantile, α , we will have our desired credible region. So we first set α equal to the tail bound,

$$(4.51) \quad \alpha = 2 \exp\left(-\frac{Cp\lambda}{2M_{k-\lambda+1}^4(1+\log(\lambda))} \min\left(\epsilon^2, \frac{\epsilon}{\omega}\right)\right),$$

and solve for ϵ , which supplies ϵ to be

$$(4.52) \quad \max \left(\sqrt{2 \log(2/\alpha) \frac{M_{k-\lambda+1}^4 (1 + \log(\lambda))}{Cp\lambda}}, 2 \log(2/\alpha) \frac{M_{k-\lambda+1}^4 (1 + \log(\lambda))\omega}{Cp\lambda} \right). \quad \blacksquare$$

We finish this subsection by describing the methodology by which to derive the stopping condition. The process will be the same for both types of errors; thus, we will show the proof only for the first error type, which corresponds to stopping too late.

Corollary 4.11. *Let $\xi_I, \xi_{II}, \delta_I \in (0, 1)$, $\delta_{II} > 1$ and $v > 0$. Under the conditions of Theorem 4.7, the following statements are true.*

$$(4.53) \quad \begin{aligned} M_{k-\lambda+1}^4 &\leq \frac{Cp\lambda \min\{(1 - \delta_I)^2 v^2, (1 - \delta_I)v/\omega\}}{(1 + \log(\lambda)) \log(2/\xi_I)} \Rightarrow \\ &\mathbb{P} \left[\tilde{\rho}_{k+1}^\lambda > v, \rho_k^\lambda \leq \delta_I v \middle| \mathcal{F}_{k-\lambda+1} \right] < \xi_I, \end{aligned}$$

and

$$(4.54) \quad \begin{aligned} M_{k-\lambda+1}^4 &\leq \frac{Cp\lambda \min\{(\delta_{II} - 1)^2 v^2, (\delta_{II} - 1)v/\omega\}}{(1 + \log(\lambda)) \log(2/\xi_{II})} \Rightarrow \\ &\mathbb{P} \left[\tilde{\rho}_{k+1}^\lambda \leq v, \rho_k > \delta_{II} v \middle| \mathcal{F}_{k-\lambda+1} \right] < \xi_{II}. \end{aligned}$$

Proof. First,

$$(4.55) \quad \begin{aligned} &\mathbb{P} \left(\tilde{\rho}_k^\lambda > v, \rho_k^\lambda \leq \delta_I v \middle| \mathcal{F}_{k-\lambda+1} \right) \\ &\leq \mathbb{P} \left(\tilde{\rho}_k^\lambda - \rho_k^\lambda > v(1 - \delta_I), \rho_k^\lambda \leq \delta_I v \middle| \mathcal{F}_{k-\lambda+1} \right) \end{aligned}$$

$$(4.56) \quad \leq \mathbb{P} \left(\tilde{\rho}_k^\lambda - \rho_k^\lambda > v(1 - \delta_I) \middle| \mathcal{F}_{k-\lambda+1} \right).$$

Using the sub-Exponential variance from Theorem 4.8 and the tail bound result from [28, Proposition 2.9],

$$(4.57) \quad \begin{aligned} &\mathbb{P} \left(\tilde{\rho}_k^\lambda - \rho_k^\lambda > v(1 - \delta_I) \middle| \mathcal{F}_{k-\lambda+1} \right) \leq \\ &\exp \left(-\frac{Cp\lambda}{2M_{k-\lambda+1}^4 (1 + \log(\lambda))} \min \left(v^2 (1 - \delta_I)^2, \frac{v(1 - \delta_I)}{\omega} \right) \right). \end{aligned}$$

Thus, when $M_{k-\lambda+1} = \|A^\top B^{1/2}\|_2 \|\mathcal{P}B^{1/2}r_{k-\lambda+1}\|_2$ satisfies the hypothesis in (4.53), the right-hand side of the preceding inequality is bounded by ξ_I . We can repeat this argument to show that (4.54) is true. \blacksquare

4.3. Estimating the Credible Interval and Stopping Condition. Corollaries 4.10 and 4.11 provide a well-controlled uncertainty set and stopping condition, yet require knowing $M_{k-\lambda+1}$, which is usually not available. As stated before, Corollaries 4.10 and 4.11 can be operationalized by replacing $M_{k-\lambda+1}^4$ with $\tilde{\iota}_k^\lambda$. Of course, $M_{k-\lambda+1}^4$ and $\tilde{\iota}_k^\lambda$ must coincide in some sense in order for this estimation to be valid. Indeed, by Theorems 4.7 and 4.9, both $M_{k-\lambda+1}^4$ and $\tilde{\iota}_k^\lambda$ converge to zero as $k \rightarrow \infty$, which would allow us to estimate $M_{k-\lambda+1}^4$ with $\tilde{\iota}_k^\lambda$ to generate consistent estimators. However, we could also estimate $M_{k-\lambda+1}^4$ by 0 to generate consistent estimators, but these would be uninformative during finite time. Therefore, we must establish that estimating $M_{k-\lambda+1}^4$ by $\tilde{\iota}_k^\lambda$ is also appropriate within some finite time. In the next result, we establish that the relative error between $M_{k-\lambda+1}^4$ and $\tilde{\iota}_k^\lambda$ is controlled by a constant (in probability).

Lemma 4.12. *Under the conditions of Theorem 4.7, for $\epsilon > 0$, $M_{k-\lambda+1}^4$ as described in Theorem 4.8, $\tilde{\iota}_k^\lambda$ as defined in (3.9),*

$$(4.58) \quad \begin{aligned} & \mathbb{P} \left(\left| \frac{M_{k-\lambda+1}^4 - \tilde{\iota}_k^\lambda}{M_{k-\lambda+1}^4} \right| > 1 + \epsilon, M_{k-\lambda+1}^4 \neq 0 \middle| \mathcal{F}_{k-\lambda+1} \right) \\ & \leq (1 + \lambda) \exp \left(- \frac{\epsilon^2 C p \lambda}{2 \left(2 + \left(\frac{\epsilon^2 \lambda}{1 + \log(\lambda)} \right)^{1/4} \right)^2 (1 + \log(\lambda))} \right). \end{aligned}$$

Proof. First,

$$(4.59) \quad \left| \frac{M_{k-\lambda+1}^4 - \tilde{\iota}_k^\lambda}{M_{k-\lambda+1}^4} \right| \leq \left| \frac{M_{k-\lambda+1}^4 - \iota_k^\lambda}{M_{k-\lambda+1}^4} \right| + \left| \frac{\iota_k^\lambda - \tilde{\iota}_k^\lambda}{M_{k-\lambda+1}^4} \right|,$$

Moreover,

$$(4.60) \quad \iota_k^\lambda \in \left[\sigma_{\min}(A^\top B^{1/2})^4 \|\mathcal{P}B^{1/2}r_k\|_2^4, M_{k-\lambda+1}^4 \right].$$

Applying this fact to (4.59),

$$(4.61) \quad \left| \frac{M_{k-\lambda+1}^4 - \tilde{\iota}_k^\lambda}{M_{k-\lambda+1}^4} \right| \leq 1 + \left| \frac{\iota_k^\lambda - \tilde{\iota}_k^\lambda}{M_{k-\lambda+1}^4} \right|.$$

We now apply a relative error version of the bound in Theorem 4.9,³ which supplies

$$(4.62) \quad \begin{aligned} & \mathbb{P} \left(\left| \frac{\iota_k^\lambda - \tilde{\iota}_k^\lambda}{M_{k-\lambda+1}^4} \right| > \epsilon \middle| \mathcal{F}_{k-\lambda+1} \right) \\ & \leq (1 + \lambda) \exp \left(- \frac{\epsilon^2 C p \lambda}{2 \left(2 + \left(\frac{\epsilon^2 \lambda}{1 + \log(\lambda)} \right)^{1/4} \right)^2 (1 + \log(\lambda))} \right). \end{aligned}$$

³For a detailed derivation of relative error bound see Lemma B.1.

The result follows by combining (4.61) and (4.62). ■

Owing to Lemma 4.12, the relative error between $\tilde{\iota}_k^\lambda$ and $M_{k-\lambda+1}$ is reasonably well controlled for practical purposes. As a result, we can use $\tilde{\iota}_k^\lambda$ as a plug-in estimator for $M_{k-\lambda+1}$ in the credible interval, (4.49), to produce the estimated credible interval suggested in Line 16 of Algorithm 3.1; and we do the same for the stopping condition controls in (4.53) and (4.54) to produce the estimated stopping condition in Line 5 of Algorithm 3.1.

5. Experimental results. Here, we have two goals. First, we demonstrate the correctness of our theory using numerical simulations. Specifically, we verify the consistency of $\tilde{\rho}_k^\lambda$ and $\tilde{\iota}_k^\lambda$ (see subsection 5.1); we verify the coverage probabilities of the credible intervals (see subsection 5.2); and we verify the effectiveness and error control for the stopping condition (see subsection 5.3). Second, we compare our method to state-of-the-art methods on an inner loop of incremental 4D-Var at very large scales (see subsection 5.4).

5.1. Consistency of Esimators. To verify the consistency of our estimators, we solve 44 least squares problems (512 unknowns, 1024 equations) with coefficient matrices generated from *Matrix Depot* [29]. Each of these least squares problems is solved three times, once for each of the FJLT, Gaussian, and Achlioptas sketching methods, using an embedding dimension of $p = 20$, a narrow moving average window width of $\lambda_1 = 1$, and a wide moving average window width of $\lambda_2 = 100$ for 10,000 iterations. At each iteration, for each of the three different sketching methods and 44 matrix systems, the values of $\tilde{\rho}_k^\lambda$, $\tilde{\iota}_k^\lambda$, ρ_k^λ , and ι_k^λ are recorded. Using these values, we compute the relative error for both estimators, $\tilde{\rho}_k^\lambda$ and $\tilde{\iota}_k^\lambda$, by taking the absolute value of the difference between the value of the estimator and the value of the quantity being estimated divided by the value of the quantity being estimated. We then summarize the distribution of these relative errors by computing the 5th, 50th and 95th percentiles for both estimator types. In the top left graph of Figure 2, we plot these percentiles for the relative error of $\tilde{\rho}_k^\lambda$, $\frac{|\tilde{\rho}_k^\lambda - \rho_k^\lambda|}{\rho_k^\lambda}$; in the top right graph, we do the same for the relative error of $\tilde{\iota}_k^\lambda$, $\frac{|\tilde{\iota}_k^\lambda - \iota_k^\lambda|}{\iota_k^\lambda}$. In the bottom graph we show an example of the absolute error of $\tilde{\iota}_k^\lambda$ (black line), and that of $\tilde{\rho}_k^\lambda$ (orange line) for the solver applied to a hadamard matrix system.

As Theorems 4.8 and 4.9 show that $\tilde{\rho}_k^\lambda$ and $\tilde{\iota}_k^\lambda$ are consistent estimators, it should be the case that we see constant relative error at all percentiles of the distribution. This is exactly what we obtain when we look at the top plots in Figure 2 with all the percentiles corresponding to relative errors that fluctuate around a particular constant. Further, looking at the bottom graph we see that in terms of absolute error, when we have ρ_k^λ converge, as it does for the hadamard matrix we see that the absolute error of $\tilde{\rho}_k^\lambda$ converges as well. The same is true for when ι_k^λ converges. Overall we can see that our estimators for ρ_k^λ and ι_k^λ are quite good, and clearly consistent when the value being estimated converges.

5.2. Coverage Probability. To verify that our credible intervals have the correct coverage probabilities, we perform a two phase experiment where we solve three linear systems (256 unknowns, 512 equations) with coefficient matrices generated from the Golub, Rohess, and Wilkinson matrices found in *Matrix Depot* [29]. In the first phase, we solve these systems once for 500 iterations using a Gaussian sketching matrix with an embedding dimension of

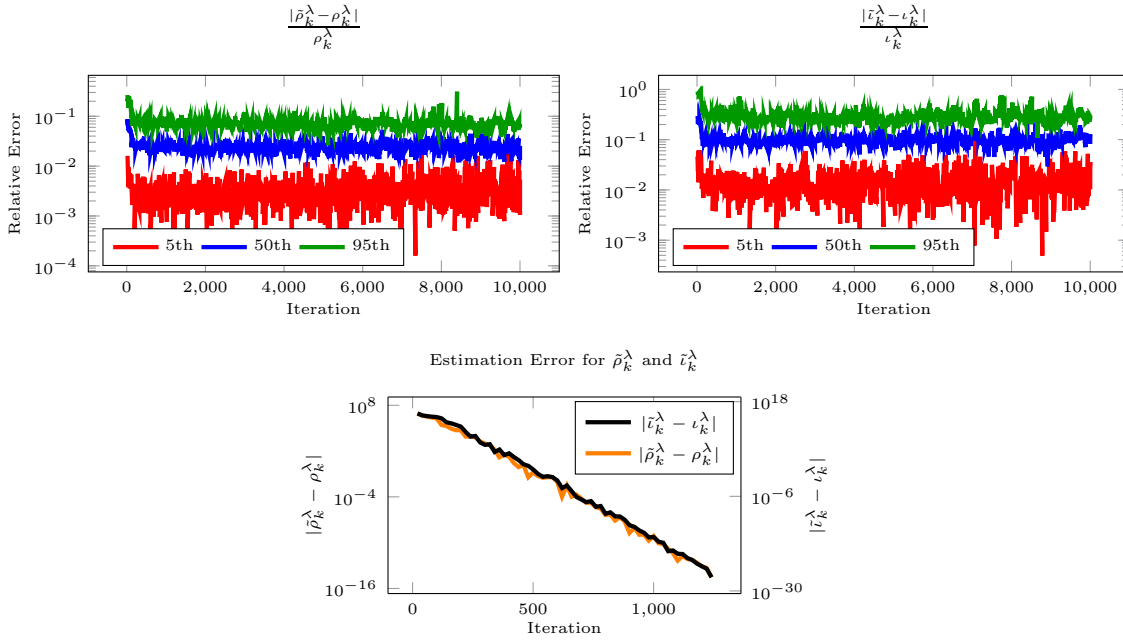


Figure 2. A relative error plot of the 5th (red), 50th (blue), and 95th (green) percentiles of the relative error between the estimator and actual value. The top left plot features the relative error of $\tilde{\rho}_k^\lambda$ across 44 least squares problems solved three times, once using each of the Gaussian, Achlioptas, and FJLT sketching methods. The top right plot features the relative error of \tilde{i}_k^λ for those same problems. The bottom plot features the absolute error for $\tilde{\rho}_k^\lambda$ and \tilde{i}_k^λ when applied to a hadamard matrix.

$p = 25$ and a constant moving average window width of $\lambda = 15$. At each iteration during this phase, we save the iterate, $\{x_k\}$, $\tilde{\rho}_k^\lambda$, and the 95% credible interval. Once the first phase is complete we move onto the second phase. In the second phase, we use the first phase's iterates as starting points from which we run [Algorithm 3.1](#) for 15 iterations, 1000 independent times, saving the true norm of the gradient, $\|g_k\|_2$, at each iteration. At the end of each 15 iteration run, we compute ρ_k^λ for that run, resulting in a set of 1000 different possible ρ_k^λ values for every iteration greater than or equal to 15. Doing this results in an approximation of the variability of ρ_k^λ at iteration k conditioned on $\mathcal{F}_{k-\lambda+1}$ as required by [Theorem 4.8](#). We then use this approximate variability to determine how often the first phase's 95% credible interval fails to cover the ρ_k^λ s.

In [Figure 3](#), we display for each iteration, k , the credible interval bounds, black lines, shifted by subtracting the first phase's $\tilde{\rho}_k^\lambda$ s, resulting in an interval centered at zero. Additionally, for each iteration, we display $\rho_k^\lambda - \tilde{\rho}_k^\lambda$ for each of the second phase's 1000 different ρ_k^λ s. If the difference is within the credible interval bound, the point is colored green otherwise it is colored red. In the left-hand plots of [Figure 3](#) we display the results for when the credible interval is computed with $\eta = 1$, while the right-hand plots display the results for a credible interval computed with η according to [Table 3](#).

From [Figure 3](#), we can see that with $\eta = 1$ the credible intervals are very conservative, with all three matrices having a coverage failure rate of zero, far more conservative than the

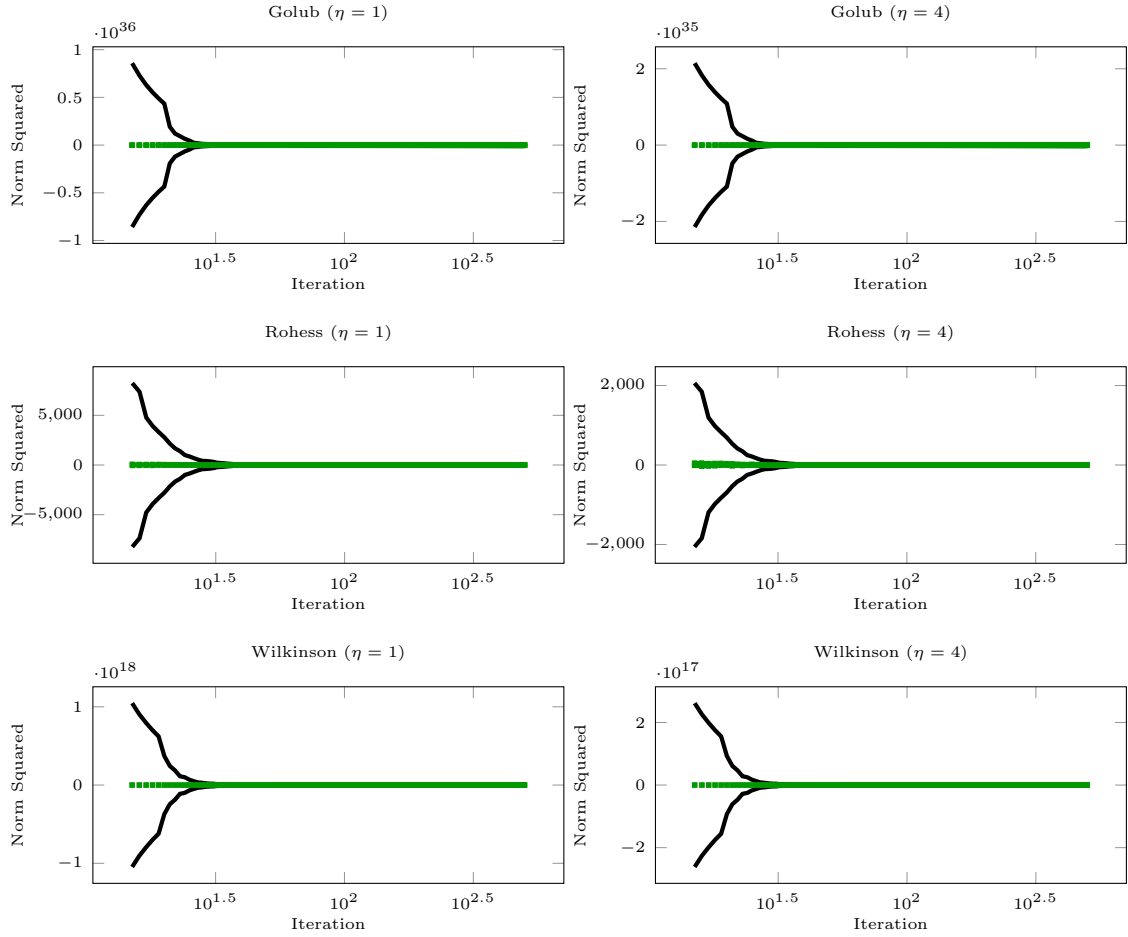


Figure 3. Coverage results for credible intervals with $\alpha = 0.05$. The plots on the left display the coverage when the credible interval is calculated with $\eta = 1$, while those on the right are computed with η chosen according to Table 3. The green points display all the values of ρ_k^λ that remain within the interval, while the red points are the values of ρ_k^λ that fall outside the interval. The failure rates when $\eta = 1$ for the Golub, Rohess, and Wilkinson matrices are $(0, 0, 0)$ respectively, while when the η parameter is set according to Table 3 these values change to $(0, 0.00000206, 0)$.

0.05 failure rate for which the interval was designed. With the η parameter chosen according to Table 3, we observe less conservative coverage rates across different systems. With the highest frequency of coverage failure being 0.00000206 for the Rohess matrix and the lowest coverage failure rate remaining 0 for the other two problems. These results emphasize that the choice of η according to Table 3 is still a conservative choice, and could possibly be chosen more aggressively based on matrix properties. Overall these results indicate that our credible intervals, while conservative, behave in a way that aligns with our theory.

5.3. Stopping Condition. To determine the effectiveness of the stopping condition we again consider 44 least squares problems (512 unknowns, 1024 equations) with coefficient matrices generated from *Matrix Depot* [29]. Each of these least squares problems is solved

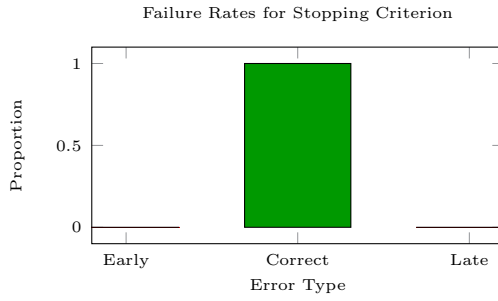


Figure 4. Graph depicting the stopping decision results by error type. The late category describes an error of the form (4.53), while early describes an error of the form (4.54). These results are displayed with $\eta = 1$; however, they remain unchanged even if η is chosen according to Table 3.

three times with once for each of the FJLT, Gaussian, and Achlioptas sketching methods with an embedding dimension of $p = 20$, a narrow moving average window width of $\lambda_1 = 1$, and a wide moving average window width of $\lambda_2 = 100$ for 10,000 iterations. After solving these systems, we then consider the frequency at which stopping errors of the form of (4.53) and (4.54) occur when the condition,

$$\tilde{\rho}_k^\lambda \leq \min \left\{ \frac{Cp\lambda\eta \min\{(1 - \delta_I)^2 v^2, (1 - \delta_I)v/\omega\}}{(1 + \log(\lambda)) \log(2/\xi_I)}, \frac{Cp\lambda\eta \min\{(\delta_{II} - 1)^2 v^2, (\delta_{II} - 1)v/\omega\}}{(1 + \log(\lambda)) \log(2/\xi_{II})} \right\},$$

is satisfied. We do this by considering all iterations where (5.1) is satisfied, then determining the frequency that (4.53) —stopping too late—occurs in these iterations, as well as how often (4.54) —stopping too early—occurs in this set of iterations. The parameters $(v, \delta_I, \delta_{II}, \xi_I, \xi_{II})$ are set to be $(100, 0.9, 1.1, 0.01, 0.01)$.

Looking at the Figure 4, we observe that when (5.1) is satisfied, no error of the form (4.53) nor (4.54) occurs, and this continues to be the case even with η set according to Table 3. This low failure rate indicates that overall (5.1), effectively controls the stopping errors. Thus, if we stop when both $\tilde{\rho}_k^\lambda \leq v$ and (5.1) occur, we will make a stopping decision with a magnitude and error rate acceptable to the user.

5.4. 4D-Variational Data Assimilation. To demonstrate the utility of Algorithm 3.1, we consider the Incremental 4D-Variational Data Assimilation problem, 4D-Var [4]. This problem is solved by iteratively updating an initial estimate by minimizing the distance between noisy observations at different time points and predictions of these observations made by evolving an estimate of the initial state to the same points in time as the observations. To evolve the initial state for our experiment, we use the dynamics defined by the one dimensional Shallow Water Equations, which are,

$$(5.1) \quad \frac{\partial \phi(x, t)}{\partial t} = -\frac{\partial}{\partial x} \phi(x, t) u(x, t),$$

and

$$(5.2) \quad \frac{\partial u(x, t)}{\partial t} = -\frac{\partial}{\partial x} \left(\phi(x, t) + \frac{u(x, t)^2}{2} \right),$$

where x is the spatial coordinate, t is the time point, $\phi(x, t)$ is the potential energy, and $u(x, t)$ is the velocity[6].

To solve a 4D-Var problem with these Shallow Water dynamics, rather than directly considering [Algorithm 3.1](#), we consider a modified version of [Algorithm 3.1](#), [Algorithm C.1](#), specifically tailored to the 4D-Var problem in a way that minimizes memory usage, and compare it to the LSQR solver [17] applied to the same system. For this comparison, we first demonstrate on small problems, those less than 32 GB in size, how [Algorithm C.1](#) produces the same quality of solution as LSQR, has the same runtime scaling as LSQR, and uses substantially less memory than LSQR, when we vary either the number of time points or the number of coordinate points and keep the other at a constant size. We then show the capabilities of [Algorithm C.1](#) exceed those of LSQR, by solving a 4D-Var problem where the system size at 0.78 TB far exceeds 32 GB memory constraint.

To perform both experiments, we generate a set of observations of the potential energy and velocity states for the Shallow Water equations with the desired number of time and coordinate points. This is done using Euler's method with the initial condition of potential energy being set to $\frac{(i-100)^2}{10000}$, where i is the index of the location, and the initial condition on velocity being set to 0.5 for all coordinates. Each time point is set to be 10^{-11} units apart and each coordinate point is 100 units apart to ensure that the system can be stably simulated when the number of coordinates and time points is large. Since in most practical instances, one would only observe either the potential energy or velocity at a particular location, we set all velocity components of the observations to zero. We then add a vector with mean zero, variance one, Gaussian entries to the potential energy states at each time point, which results in our noisy solutions.⁴

With these observations, we then solve a single inner iteration of the Incremental 4D-Var problem with an initial state estimate of $\frac{(j-100)^4}{10000}$, where j is the entry index of the state vector, once with LSQR and once with [Algorithm C.1](#). For [Algorithm C.1](#), we use the Achlioptas sketching method with an embedding dimension of $p = 20$, a narrow moving average window width of $\lambda_1 = 1$, a wide moving average window width of $\lambda_2 = 100$. In order to account for the floating point errors associated with solving large matrix systems, the threshold for stopping is set to be $v = 10^{-9}(N_c(N_t+1))$, where N_c is the number of coordinates and N_t is the number of time points. The other stopping parameters, $(\delta_I, \delta_{II}, \xi_I, \xi_{II})$ are set to be $(.9, 1.1, .95, .95)$. For both solvers we use a single thread of an Intel Xeon E5-2680 v3 @ 2.50GHz with a memory constraint of 32 GB. We consider systems with the number time points varying from 20 to 640 by way of doubling, as well as with the number of coordinate points varying from 20 to 1280 by way of doubling. This results in matrix systems that range in size from 250 KB to 31.25 GB. The LSQR algorithm is stopped once an absolute error of v is achieved and [Algorithm C.1](#) is stopped according to Line 2 of [Algorithm 3.1](#). Once stopped, we compare the runtime scaling, memory usage, and norm squared of the residual of final solution for both

⁴Precise formulations of the equations used for Euler's method can be found in [Appendix C](#).

methods in the cases where the number of coordinates change, but number time points stay constant and vice versa.

The results for keeping the number of time points constant at 640 and varying the number of coordinates are displayed on the left of [Figure 5](#), and the results for keeping the number of coordinates constant at 1280 and varying the number of time points are displayed on the right of [Figure 5](#). In all instances, the minimum residual found by both methods is the same. When considering runtime, the runtime for the LSQR method is faster than [Algorithm C.1](#), as long as the matrix system size is less than the memory constraint, and if the system size is greater than the memory constraint, the LSQR method fails. Since we care most about how the methods scale with changes in the number of coordinates or number of time points, we present how many times longer the runtime of the solver is at a particular system size, compared to the runtime of the same solver applied to a system with half as many coordinate or time points.

Looking at both sets of plots, we see that for a fixed time point, the LSQR method and [Algorithm C.1](#) increase at close to the same rate with LSQR taking on average 4.57 times longer to solve a problem with twice as many coordinates and [Algorithm C.1](#) taking 5 times longer to solve a problem with twice as many coordinates. This trend continues until we reach the system with 1280 coordinate points, at which point the LSQR runtime is 70 times longer than it was at 640 coordinate points, while [Algorithm C.1](#) only takes 4.46 times longer. Evidence for why [Algorithm C.1](#) does not experience the same scaling issues as LSQR is found in the memory frame of [Figure 5](#) where we observe the memory usage for [Algorithm C.1](#) remains relatively constant at every value of the number of coordinate points, while the memory usage for LSQR grows quadratically over the same span, reaching a maximum of 31.5 GB of memory used. A similar story can be observed if we vary the number of time points, with [Algorithm C.1](#) and LSQR algorithm both doubling in runtime for every doubling in the number of time points, until 640 time points are reached, at which point the scaling for LSQR becomes 37 times that of the previous system size, but remains constant for [Algorithm C.1](#). In all we, can conclude that to generate the same solution quality, [Algorithm C.1](#) scales as well as LSQR with a longer overall runtime, but is significantly more memory efficient than LSQR and is therefore able to avoid the poor memory scaling for longer than LSQR.

We finally consider the sketched residual and credible interval for a Shallow Water problem with 250 time points and 10240 spatial coordinates, which equates to a system with a storage requirement of 0.78 TB. We use Achlioptas sketching with an embedding dimension of $p = 20$, a narrow moving average window width of $\lambda_1 = 1$, and a wide moving average window width of $\lambda_2 = 100$. As with the previous problem we solve this system using a single thread of an Intel Xeon E5-2680 v3 @ 2.50GHz with a memory constraint of 32 GB of which [Algorithm C.1](#) uses 194.68 MB.

We observe in [Figure 6](#) that most of the progress is made within the first 100,000 iterations progressing from a $\tilde{\rho}_k^\lambda$ value of 1.466019×10^{32} to a value of 6520.793. The likely cause for this stalled progress is the conditioning of the system, since even at larger sample sizes, $\tilde{\rho}_k^\lambda$ does not improve beyond 6520.793. This leads us to claim we have solved the system sufficiently, and have done so under constraints for which LSQR fails to work.

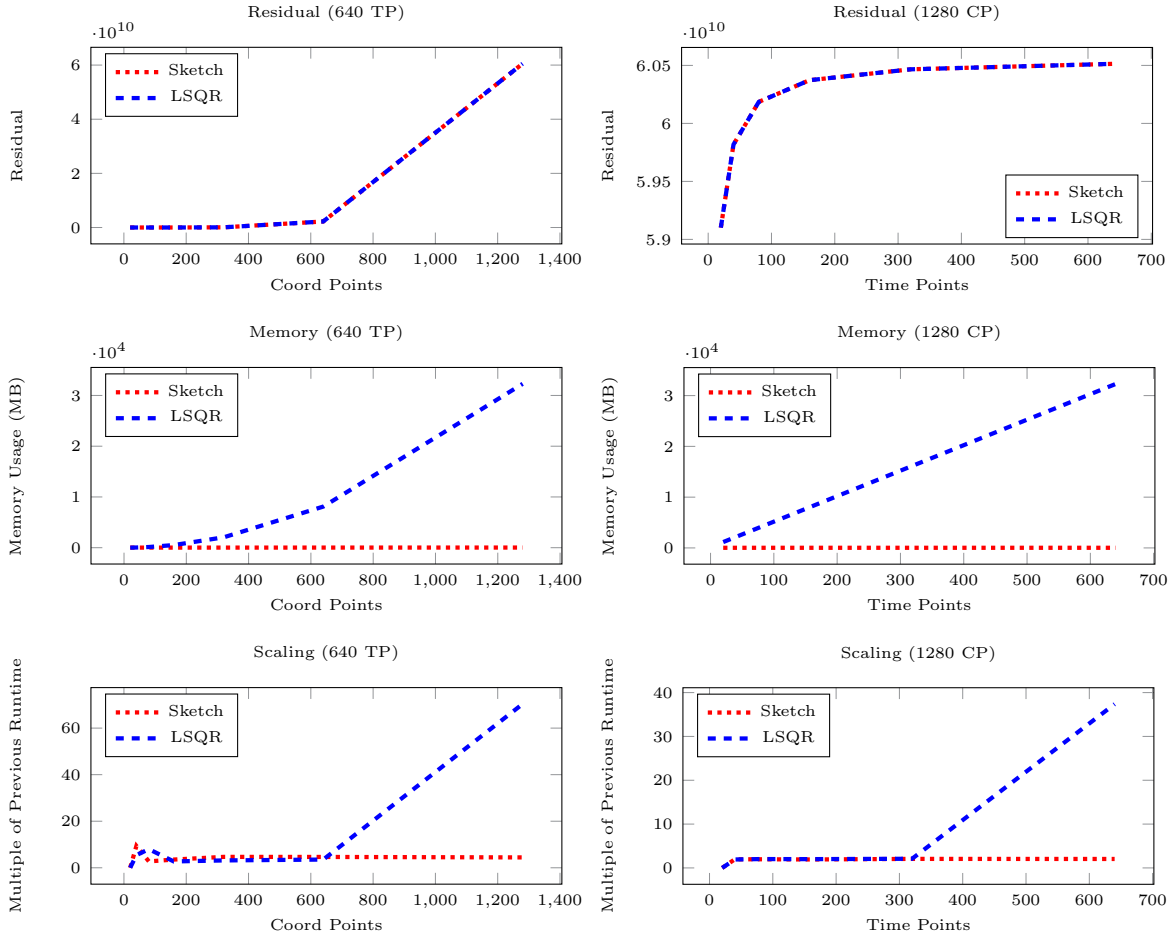


Figure 5. Displays how residual (top), memory (middle), and slowdown (bottom) compare between LSQR and [Algorithm C.1](#). The left graphs show scaling when the time points (TP) are set at 640 and the number of coordinates are allowed to vary. The right graphs show scaling when the coordinate points (CP) are set at 1280 and number of time points are allowed to vary. The blue curve shows the results for the LSQR solver while the red line shows the results for our solver implemented with [Algorithm C.1](#).

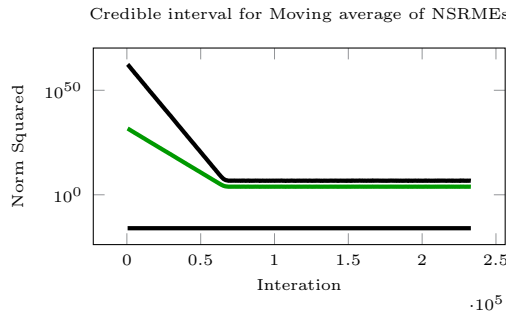


Figure 6. Displays $\hat{\rho}_k^\lambda$ and the credible interval for the single inner iteration solve of the large 4D-Var system which has 10240 spatial coordinates and 250 time points. It should be noted that for better viewing of the trend in progress, we set the lower bound to be 10^{-16} at the iterations where it was negative.

6. Conclusions. To efficiently solve the large-scale least squares subproblems that arise in uncertainty quantification, such as 4D-Var, we have proposed an iterative method that leverages random sketching to solve these least squares problems with minimal memory load. The iterative nature of our solution leads to a need to track and stop our method with minimal computational cost, a goal we achieve by utilizing the moving average of the sketched gradients. Through our rigorous proofs, we are then able to verify that not only does our algorithm converge, but also that our estimators are consistent and have a quantifiable uncertainty despite their dependent structure. We perform numerous numerical experiments to verify that this theory holds in practice. In addition to the practical verification of our theory, we make clear the advantages of our method over one like LSQR by comparing both solvers on a 0.78 TB system. Through this comparison we find that while the LSQR method fails due to reaching the 32 GB memory bound, our method can solve the system utilizing only 195 MB of memory. Our future work will involve improving the practicality of our methodology for solving large-scale scientific problems by examining the effects of the choice of embedding dimension on convergence rate and considering parallelization opportunities to reduce runtime.

Appendix A. Commutation of Projection Matrices. We begin by proving that when one orthogonal projection matrix projects onto a space that is a subset of the space projected onto by a second orthogonal projection matrix, the matrices commute. This allows for us to make the conclusion in (4.5).

Lemma A.1. *If \mathcal{P}_A is an orthogonal projection matrix onto the range of A and \mathcal{P}_{AB} is an orthogonal projection matrix onto the range of AB , then it is the case*

$$(A.1) \quad \mathcal{P}_A \mathcal{P}_{AB} = \mathcal{P}_{AB} \mathcal{P}_A.$$

Proof. We begin by noting that any orthogonal projection matrix P has an eigen decomposition of the following form,

$$(A.2) \quad P = U \Lambda U',$$

where U is an orthonormal matrix whose rows span the range of P and if we let $n = \text{Dim}(P)$, then $\Lambda = \begin{bmatrix} I_n & 0 \\ 0 & 0 \end{bmatrix}$. Since $\text{range}(AB) \subseteq \text{range}(A)$, we can define U_1 to be the orthonormal matrix whose rows span $\text{range}(AB)$, let U_2 be the orthonormal matrix whose rows span $\text{range}(A)$ but not $\text{range}(AB)$, and let U_3 be the orthonormal matrix with rows span the Nullspace(A). With these matrices defined we can now decompose the two projection matrices as

$$(A.3) \quad \mathcal{P}_{AB} = \begin{bmatrix} U_1 \\ U_2 \\ U_3 \end{bmatrix} \begin{bmatrix} I_r & 0 & 0 \\ 0 & 0_s & 0 \\ 0 & 0 & 0_w \end{bmatrix} \begin{bmatrix} U_1 \\ U_2 \\ U_3 \end{bmatrix}',$$

and

$$(A.4) \quad \mathcal{P}_A = \begin{bmatrix} U_1 \\ U_2 \\ U_3 \end{bmatrix} \begin{bmatrix} I_r & 0 & 0 \\ 0 & I_s & 0 \\ 0 & 0 & 0_w \end{bmatrix} \begin{bmatrix} U_1 \\ U_2 \\ U_3 \end{bmatrix}',$$

where $r = \dim(\text{range}(BA))$ and $s = \dim(\text{range}(A) - \text{range}(BA))$. Using these definitions then have

$$(A.5) \quad \mathcal{P}_A \mathcal{P}_{AB} = \begin{bmatrix} U_1 \\ U_2 \\ U_3 \end{bmatrix} \begin{bmatrix} I_r & 0 & 0 \\ 0 & I_s & 0 \\ 0 & 0 & 0 \end{bmatrix} \begin{bmatrix} I_r & 0 & 0 \\ 0 & 0 & 0 \\ 0 & 0 & 0 \end{bmatrix} \begin{bmatrix} U_1 \\ U_2 \\ U_3 \end{bmatrix}'$$

$$(A.6) \quad = \begin{bmatrix} U_1 \\ U_2 \\ U_3 \end{bmatrix} \begin{bmatrix} I_r & 0 & 0 \\ 0 & 0 & 0 \\ 0 & 0 & 0 \end{bmatrix} \begin{bmatrix} I_r & 0 & 0 \\ 0 & I_s & 0 \\ 0 & 0 & 0 \end{bmatrix} \begin{bmatrix} U_1 \\ U_2 \\ U_3 \end{bmatrix}'$$

$$(A.7) \quad = \mathcal{P}_{AB} \mathcal{P}_A.$$

Where the first and last line use the orthogonality of the U_i matrices and the second line uses the fact that diagonal matrices commute. \blacksquare

Appendix B. Relative error bound for ι_k^λ . Here we define the relative error bound used at the end of the proof of [Lemma 4.12](#), which is simply a relative error version of [Theorem 4.9](#). We present the exact derivation of this bound in the following lemma.

Lemma B.1. *Under the conditions of [Theorem 4.7](#), we have*

$$(B.1) \quad \mathbb{P} \left(\left| \tilde{\iota}_k^\lambda - \iota_k^\lambda \right| > \epsilon \right) \leq (1 + \lambda) \exp \left(- \frac{\epsilon^2 C p \lambda}{2 \left(2 + \left(\frac{\epsilon^2 \lambda}{(1 + \log(\lambda))} \right)^{1/4} \right)^2 (1 + \log(\lambda))} \right)$$

Proof. Using the definitions of ι_k^λ and $\tilde{\iota}_k^\lambda$ we have

$$(B.2) \quad \mathbb{P} \left(\left| \frac{\tilde{\iota}_k^\lambda - \iota_k^\lambda}{M_{k-\lambda+1}^4} \right| > \epsilon \middle| \mathcal{F}_{k-\lambda+1} \right)$$

$$(B.3) \quad = \mathbb{P} \left(\left| \sum_{i=k-\lambda+1}^k \frac{\|\tilde{g}_i\|_2^4 - \|g_i\|_2^4}{\lambda M_{k-\lambda+1}^4} \right| > \epsilon \middle| \mathcal{F}_{k-\lambda+1} \right)$$

$$(B.4) \quad \leq \mathbb{P} \left(\sum_{i=k-\lambda+1}^k \left| \frac{\|\tilde{g}_i\|_2^4 - \|g_i\|_2^4}{\lambda M_{k-\lambda+1}^4} \right| > \epsilon \middle| \mathcal{F}_{k-\lambda+1} \right)$$

$$(B.5) \quad \leq \mathbb{P} \left(\sum_{i=k-\lambda+1}^k \left| \frac{\|\tilde{g}_i\|_2^2 - \|g_i\|_2^2}{\lambda M_{k-\lambda+1}^2} \right| \left| \frac{\|\tilde{g}_i\|_2^2 + \|g_i\|_2^2}{M_{k-\lambda+1}^2} \right| > \epsilon \middle| \mathcal{F}_{k-\lambda+1} \right).$$

Then by defining a variable, $G > 2$, to partition [\(B.5\)](#) into disjoint sets and using the definition of measure,

$$(B.6) \quad \mathbb{P} \left(\sum_{i=k-\lambda+1}^k \left| \frac{\|\tilde{g}_i\|_2^2 - \|g_i\|_2^2}{\lambda M_{k-\lambda+1}^2} \right| \left| \frac{\|\tilde{g}_i\|_2^2 + \|g_i\|_2^2}{M_{k-\lambda+1}^2} \right| > \epsilon \middle| \mathcal{F}_{k-\lambda+1} \right)$$

$$\begin{aligned}
(B.7) \quad &= \mathbb{P} \left(\sum_{i=k-\lambda+1}^k \left| \frac{\|\tilde{g}_i\|_2^2 - \|g_i\|_2^2}{\lambda M_{k-\lambda+1}^2} \right| \left| \frac{\|\tilde{g}_i\|_2^2 + \|g_i\|_2^2}{M_{k-\lambda+1}^2} \right| > \epsilon, \right. \\
&\quad \left. \bigcap_{i=k-\lambda+1}^k \left\{ \left| \frac{\|\tilde{g}_i\|_2^2 + \|g_i\|_2^2}{M_{k-\lambda+1}^2} \right| \leq G \right\} \middle| \mathcal{F}_{k-\lambda+1} \right) \\
&+ \mathbb{P} \left(\sum_{i=k-\lambda+1}^k \left| \frac{\|\tilde{g}_i\|_2^2 - \|g_i\|_2^2}{\lambda M_{k-\lambda+1}^2} \right| \left| \frac{\|\tilde{g}_i\|_2^2 + \|g_i\|_2^2}{M_{k-\lambda+1}^2} \right| > \epsilon, \right. \\
&\quad \left. \bigcup_{i=k-\lambda+1}^k \left\{ \left| \frac{\|\tilde{g}_i\|_2^2 + \|g_i\|_2^2}{M_{k-\lambda+1}^2} \right| > G \right\} \middle| \mathcal{F}_{k-\lambda+1} \right) \\
(B.8) \quad &\leq \mathbb{P} \left(\sum_{i=k-\lambda+1}^k \left| \frac{\|\tilde{g}_i\|_2^2 - \|g_i\|_2^2}{\lambda M_{k-\lambda+1}^2} \right| > \frac{\epsilon}{G} \middle| \mathcal{F}_{k-\lambda+1} \right) \\
&+ \mathbb{P} \left(\bigcup_{i=k-\lambda+1}^k \left\{ \left| \frac{\|\tilde{g}_i\|_2^2 + \|g_i\|_2^2}{M_{k-\lambda+1}^2} \right| > G \right\} \middle| \mathcal{F}_{k-\lambda+1} \right).
\end{aligned}$$

From here we will present the bounds for the left and right terms of (B.8) separately. For the left term of (B.8) we use (4.20) and have

$$(B.9) \quad \mathbb{P} \left(\sum_{i=k-\lambda+1}^k \left| \frac{\|\tilde{g}_i\|_2^2 - \|g_i\|_2^2}{\lambda M_{k-\lambda+1}^2} \right| > \frac{\epsilon}{G} \middle| \mathcal{F}_{k-\lambda+1} \right) \leq \exp \left(\frac{t^2(1 + \log(\lambda))}{2Cp\lambda} - \frac{\epsilon t}{G} \right)$$

$$(B.10) \quad \leq \exp \left(-\frac{\epsilon^2 C p \lambda}{2G^2(1 + \log(\lambda))} \right),$$

where (B.10) comes from minimizing (B.9) in terms of t . We next address the right side of (B.8) for which we have

$$(B.11) \quad \mathbb{P} \left(\bigcup_{i=k-\lambda+1}^k \left\{ \left| \frac{\|\tilde{g}_i\|_2^2 + \|g_i\|_2^2}{M_{k-\lambda+1}^2} \right| > G \right\} \middle| \mathcal{F}_{k-\lambda+1} \right)$$

$$(B.12) \quad = \mathbb{P} \left(\bigcup_{i=k-\lambda+1}^k \left\{ \left| \frac{\|\tilde{g}_i\|_2^2 - \|g_i\|_2^2 + 2\|g_i\|_2^2}{M_{k-\lambda+1}^2} \right| > G \right\} \middle| \mathcal{F}_{k-\lambda+1} \right)$$

$$(B.13) \quad \leq \mathbb{P} \left(\bigcup_{i=k-\lambda+1}^k \left\{ \left| \frac{\|\tilde{g}_i\|_2^2 - \|g_i\|_2^2}{M_{k-\lambda+1}^2} \right| + 2 > G \right\} \middle| \mathcal{F}_{k-\lambda+1} \right)$$

$$(B.14) \quad \leq \sum_{i=k-\lambda+1}^k \mathbb{P} \left(\left| \frac{\|\tilde{g}_i\|_2^2 - \|g_i\|_2^2}{M_{k-\lambda+1}^2} \right| > G - 2 \middle| \mathcal{F}_{k-\lambda+1} \right)$$

$$(B.15) \quad \leq \lambda \exp \left(\frac{t^2}{2Cp} - t(G - 2) \right)$$

$$(B.16) \quad \leq \lambda \exp \left(-\frac{Cp(G-2)^2}{2} \right),$$

where (B.13) comes from (4.28), (B.15) comes from the (4.20), and (B.16) comes from minimizing (B.15) in terms of t . Putting both parts together gives us,

$$(B.17) \quad \mathbb{P} \left(\left| \frac{\tilde{\iota}_k^\lambda - \iota_k^\lambda}{M_{k-\lambda+1}^4} \right| > \epsilon \middle| \mathcal{F}_{k-\lambda+1} \right)$$

$$(B.18) \quad \leq \inf_{G>2} \exp \left(-\frac{\epsilon^2 Cp\lambda}{2G^2(1+\log(\lambda))} \right) + \lambda \exp \left(-\frac{Cp(G-2)^2}{2} \right).$$

We can then observe that when $G \geq 2 + \left(\frac{\epsilon^2 \lambda}{(1+\log(\lambda))} \right)^{1/4}$ it is the case that

$$(B.19) \quad \exp \left(-\frac{\epsilon^2 Cp\lambda}{2G^2(1+\log(\lambda))} \right) \geq \exp \left(-\frac{Cp(G-2)^2}{2} \right).$$

Thus, if we let $Y = 2 + \left(\frac{\epsilon^2 \lambda}{(1+\log(\lambda))} \right)^{1/4}$ we can upper bound the right-hand side of (B.18) in the following manner,

$$(B.20) \quad \inf_{G>2} \exp \left(-\frac{\epsilon^2 Cp\lambda}{2G^2(1+\log(\lambda))} \right) + \lambda \exp \left(-\frac{Cp(G-2M_{k-\lambda+1}^2)^2}{2} \right)$$

$$(B.21) \quad \leq \inf_{G>Y} (1+\lambda) \exp \left(-\frac{\epsilon^2 Cp\lambda}{2G^2(1+\log(\lambda))} \right)$$

$$(B.22) \quad \leq (1+\lambda) \exp \left(-\frac{\epsilon^2 Cp\lambda}{2 \left(2 + \left(\frac{\epsilon^2 \lambda}{(1+\log(\lambda))} \right)^{1/4} \right)^2 (1+\log(\lambda))} \right). \quad \blacksquare$$

Appendix C. Shallow Water Model.

For the experiment in subsection 5.4, we use the one dimensional shallow water problem as defined in work of Dimet et al. [6], which involves solving the following system of partial differential equations:

$$(C.1) \quad \frac{\partial \phi(x, t)}{\partial t} = -\frac{\partial}{\partial x}(\phi(x, t)u(x, t))$$

and

$$(C.2) \quad \frac{\partial u(x, t)}{\partial t} = -\frac{\partial}{\partial x} \left(\phi(x, t) + \frac{u(x, t)^2}{2} \right).$$

The functions $\phi(x, t)$ and $u(x, t)$ are unknown functions of the position, x , and time point, t . The function $\phi(x, t)$ represents the potential energy at a location at a particular time, and $u(x, t)$ represents the velocity at a location at a particular time.

In this section we lay out the specifics of our 4D-Var problem by first discussing our simulation using Euler's method, then writing out our Jacobian equations used in incremental 4D-Var, before finally presenting our modified version of [Algorithm 3.1](#).

The Forward Model. To generate noisy observations to be assimilated, it is necessary to simulate the system. This simulation will be generated using a forward Euler method, which requires the discretization of the differential equations. In order to discretize the system we use Δ_t to represent an increment in time and Δ_x to indicate an increment in position. With this notation defined, the discretization of [\(C.1\)](#) is

$$(C.3) \quad \frac{\partial \phi(x, t)}{\partial t} \approx \frac{\phi(x, t + \Delta_t) - \phi(x, t)}{\Delta_t} = u(x, t) \frac{\phi(x - \Delta_x, t) - \phi(x + \Delta_x, t)}{2\Delta_x} + \phi(x, t) \frac{u(x - \Delta_x, t) - u(x + \Delta_x, t)}{2\Delta_x},$$

and the discretization of [\(C.2\)](#) is

$$(C.4) \quad \frac{\partial u(x, t)}{\partial t} \approx \frac{u(x, t + \Delta_t) - u(x, t)}{\Delta_t} = \frac{\phi(x - \Delta_x, t) - \phi(x + \Delta_x, t)}{2\Delta_x} + u(x, t) \frac{u(x - \Delta_x, t) - u(x + \Delta_x, t)}{2\Delta_x}.$$

From the discretization, we can then derive the state at a new time point for ϕ and u . Specifically, they are

$$(C.5) \quad \phi(x, t + \Delta_t) = \phi(x, t) + \Delta_t \left(u(x, t) \frac{\phi(x - \Delta_x, t) - \phi(x + \Delta_x, t)}{2\Delta_x} + \phi(x, t) \frac{u(x - \Delta_x, t) - u(x + \Delta_x, t)}{2\Delta_x} \right),$$

for ϕ and

$$(C.6) \quad u(x, t + \Delta_t) = u(x, t) + \Delta_t \left(\frac{\phi(x - \Delta_x, t) - \phi(x + \Delta_x, t)}{2\Delta_x} + u(x, t) \frac{u(x - \Delta_x, t) - u(x + \Delta_x, t)}{2\Delta_x} \right),$$

for u .

The tangent model. For incremental 4D-Var it is necessary to not only have the forward model, but also the first order linearization of that model [\[26\]](#). This linearization requires the calculation of the Jacobian of the discretized model in terms of the functions u and ϕ at all possible values of x [\[12\]](#). The nonzero Jacobian values at a particular position x are:

$$(C.7) \quad \frac{\partial \phi(x, t + \Delta_t)}{\partial \phi(x + \Delta_x, t)} = -\frac{\Delta_t}{2\Delta_x} u(x, t),$$

$$(C.8) \quad \frac{\partial \phi(x, t + \Delta_t)}{\partial \phi(x, t)} = 1 + \Delta_t \frac{u(x - \Delta_x, t) - u(x + \Delta_x, t)}{2\Delta_x},$$

$$(C.9) \quad \frac{\partial \phi(x, t + \Delta_t)}{\partial \phi(x - \Delta_x, t)} = \frac{\Delta_t}{2\Delta_x} u(x, t),$$

$$(C.10) \quad \frac{\partial \phi(x, t + \Delta_t)}{\partial u(x + \Delta_x, t)} = -\frac{\Delta_t}{2\Delta_x} \phi(x, t),$$

$$(C.11) \quad \frac{\partial \phi(x, t + \Delta_t)}{\partial u(x, t)} = \Delta_t \frac{\phi(x - \Delta_x, t) - \phi(x + \Delta_x, t)}{2\Delta_x},$$

$$(C.12) \quad \frac{\partial \phi(x, t + \Delta_t)}{\partial u(x - \Delta_x, t)} = \frac{\Delta_t}{2\Delta_x} \phi(x, t),$$

$$(C.13) \quad \frac{\partial u(x, t + \Delta_t)}{\partial \phi(x + \Delta_x, t)} = -\frac{\Delta_t}{2\Delta_x},$$

$$(C.14) \quad \frac{\partial u(x, t + \Delta_t)}{\partial \phi(x, t)} = 0,$$

$$(C.15) \quad \frac{\partial u(x, t + \Delta_t)}{\partial \phi(x - \Delta_x, t)} = \frac{\Delta_t}{2\Delta_x},$$

$$(C.16) \quad \frac{\partial u(x, t + \Delta_t)}{\partial u(x + \Delta_x, t)} = -\frac{\Delta_t}{2\Delta_x} u(x, t),$$

$$(C.17) \quad \frac{\partial u(x, t + \Delta_t)}{\partial u(x, t)} = 1 + \Delta_t \frac{u(x - \Delta_x, t) - u(x + \Delta_x, t)}{2\Delta_x},$$

and

$$(C.18) \quad \frac{\partial u(x, t + \Delta_t)}{\partial u(x - \Delta_x, t)} = \frac{\Delta_t}{2\Delta_x} u(x, t).$$

C.1. A Reduced Memory Algorithm for 4D-Var. When solving the Incremental 4D-Variational data assimilation problem, we wish to find the incremental update u^k to an initial state estimate z^{k-1} by solving

$$(C.19) \quad \min_{u^k} \frac{1}{2} \left(\|(z^{k-1} - z_b) - u^k\|_V^2 + \sum_{i=0}^{N_t} \|H_i^{k-1} M_{0,i}^{k-1} u^k - (y_i - H_i(x_i^{k-1}))\|_W^2 \right).$$

Here V is the inverse covariance matrix for the background states, W is the inverse covariance matrix for the observations, N_t is the number of time points observed in the data, z_b is the

background state, z^{k-1} is the current state estimate, y_i is the observation at the i^{th} time point, x^{k-1} is the result of forward Euler applied to z^{k-1} from time 0 to time i , H_i^{k-1} is the Jacobian of the observation function, H_i , and $M_{0,i}^{k-1}$ is the product of Jacobian matrices of the dynamics from time point zero to time point i [8]. Under this setup, this problem can be solved using least squares solvers, and has a convenient structure that can be exploited by a row solver such that the memory load is minimized. The main structural advantage comes from us being able to generate $M_{0,i}^{k-1}$ as needed as we progress through the algorithm, meaning that by running the algorithm in a row-wise fashion and let N_s be the number of state variables, we only need to store a matrix of dimension $N_s \times N_s$ rather than $N_t N_s \times N_s$. We can additionally use right sketching to reduce the number of columns, which further reduces the storage costs to $N_s \times p$, where p is the sketch size. This substantial reduction in memory cost allows our solver to avoid substantial slowdowns from the full matrix memory accesses encounter by Krylov based methods, such as LSQR.

Due to the inherent structure of the matrix system in the 4D-Var problem and our choice of [16] as a solver, which can work on row based blocks of a matrix; we propose a modified version of [Algorithm 3.1](#), that does not require access to the full matrix system in the 4D-Var problem.

REFERENCES

- [1] D. ACHLIOPAS, *Database-friendly random projections: Johnson-lindenstrauss with binary coins*, Journal of Computer and System Sciences, 66 (2003), pp. 671–687, [https://doi.org/https://doi.org/10.1016/S0022-0000\(03\)00025-4](https://doi.org/https://doi.org/10.1016/S0022-0000(03)00025-4), <https://www.sciencedirect.com/science/article/pii/S0022000003000254>. Special Issue on PODS 2001.
- [2] N. AILON AND B. CHAZELLE, *The fast johnson-lindenstrauss transform and approximate nearest neighbors*, SIAM J. Comput., 39 (2009), pp. 302–322.
- [3] S. CHEN, X. HONG, AND C. J. HARRIS, *Sparse kernel regression modeling using combined locally regularized orthogonal least squares and d-optimality experimental design*, IEEE Transactions on Automatic Control, 48 (2003), pp. 1029–1036.
- [4] P. COURTIER, J.-N. THÉPAUT, AND A. HOLLINGSWORTH, *A strategy for operational implementation of 4d-var, using an incremental approach*, Quarterly Journal of the Royal Meteorological Society, 120 (1994), pp. 1367–1387.
- [5] S. DASGUPTA AND A. GUPTA, *An elementary proof of a theorem of johnson and lindenstrauss*, Random Struct. Algorithms, 22 (2003), pp. 60–65.
- [6] F.-X. L. DIMET AND O. TALAGRAND, *Variational algorithms for analysis and assimilation of meteorological observations: theoretical aspects*, Tellus A, 38A (1986), pp. 97–110, <https://doi.org/https://doi.org/10.1111/j.1600-0870.1986.tb00459.x>, <https://onlinelibrary.wiley.com/doi/abs/10.1111/j.1600-0870.1986.tb00459.x>, <https://arxiv.org/abs/https://onlinelibrary.wiley.com/doi/pdf/10.1111/j.1600-0870.1986.tb00459.x>.
- [7] R. DURRETT, *Probability: Theory and examples*, 2013.
- [8] S. GUROL, A. WEAVER, A. MOORE, A. PIACCENTINI, H. ARANGO, AND S. GRATTON, *B-preconditioned minimization algorithms for variational data assimilation with the dual formulation*, Quarterly Journal of the Royal Meteorological Society, 140 (2013), pp. 539–556, <https://doi.org/10.1002/qj.2150>, <https://hal.archives-ouvertes.fr/hal-03224132>.
- [9] K. HAYAMI, J.-F. YIN, AND T. ITO, *Gmres methods for least squares problems*, SIAM Journal on Matrix Analysis and Applications, 31 (2010), pp. 2400–2430, <https://doi.org/10.1137/070696313>, <https://doi.org/10.1137/070696313>, <https://arxiv.org/abs/https://doi.org/10.1137/070696313>.
- [10] P. INDYK AND R. MOTWANI, *Approximate nearest neighbors: Towards removing the curse of dimensionality*, (1998), p. 604–613, <https://doi.org/10.1145/276698.276876>, <https://doi.org/10.1145/276698>.

Algorithm C.1 Tracking and Stopping for Least Squares

Require: Random sketching method satisfying [Definition 3.1](#) and sketch size s .
Require: $V \in \mathbb{R}^{N_s \times N_s}$, $W \in \mathbb{R}^{N_s \times N_s}$ $b \in \mathbb{R}^m$, $z_0 \in \mathbb{R}^{N_s}$, $z_b \in \mathbb{R}^{N_s}$, $u_0 \in \mathbb{R}^s$, $\{y_i : i \in \{1, \dots, N_t\}\}$.
Require: Moving window size $\lambda_1 \leq \lambda_2 \in \mathbb{N}$.
Require: $\alpha > 0$, $\xi_I > 0$, $\xi_{II} > 0$, $\delta_I \in (0, 1)$, $\delta_{II} > 1$, $\eta \geq 1$, $v > 0$.
Require: Function $\mathbf{h}(\cdot)$ which applies the observation operator to a vector.
Require: Function **ForwardEuler**(\cdot) progress a state vector forward one time point.
Require: Function **Jacobian**(\cdot) generates the Jacobian matrix at a particular time point based on the state vector.

$k \leftarrow 0$, $k' \leftarrow \infty$, $\tilde{\rho}_0^* \leftarrow 0$, $\tilde{\iota}_0^* \leftarrow 0$, $\lambda_o \leftarrow 0$, $\lambda \leftarrow \lambda_1$, $\rho \leftarrow \{0\}^{\lambda_2}$, $\tilde{\iota} \leftarrow \{0\}^{\lambda_2}$, $u_k \leftarrow \{0\}^n$, $R \leftarrow \{0\}^{s \times s}$, $Tab \leftarrow \{0\}^s$, $D \leftarrow \{0\}^s$.

2: **while** $k == 0$ **or** $\tilde{\rho}_k^\lambda \geq v$ **or**

$$\tilde{\iota}_k^\lambda \geq \min \left\{ \frac{Cp\lambda\eta \min\{(1 - \delta_I)^2 v^2, (1 - \delta_I)v/\omega\}}{(1 + \log(\lambda)) \log(2/\xi_I)}, \frac{Cp\lambda\eta \min\{(\delta_{II} - 1)^2 v^2, (\delta_{II} - 1)v/\omega\}}{(1 + \log(\lambda)) \log(2/\xi_{II})} \right\}$$

do

Iteration k

4: Generate S_k and $(AS)_0 \leftarrow S_k$.

$r_0 \leftarrow u_k - z_b + z_0$

6: $\tilde{g}_k \leftarrow V(AS)_0' r_0$

Use Gentleman's, [16], on the problem $\min_{u_p} \|(AS)_0 u_p - r\|_V^2$, to update R , Tab , and D .

8: Set $evol_0 \leftarrow z_0$

for $i = 1$:ntimes **do**

10: $evol_i \leftarrow \mathbf{ForwardEuler}(evol_{i-1})$.

$M_i \leftarrow \mathbf{Jacobian}(evol_i)$.

12: $(AS)_i \leftarrow M_i(AS)_{i-1}$.

$r_k = M_i u_k - (y_i - \mathbf{h}(evol_i))$

14: $\tilde{g}_k \leftarrow \tilde{g}_{k-1} + W(AS)'_{i-1} r_k$

Use Gentleman's, [16], on $\min_{u_p} \|(AS)_k u_p - r_k\|_W^2$, to update R , Tab , and D .

16: **end for**

$u_{k+1} \leftarrow R^{-1} Tab$

18: Perform Lines 7 - 16 of [Algorithm 3.1](#).

$x_{k+1} \leftarrow x_k - S_k u_{k+1}$

20: $D \leftarrow \{0\}^s$, $Tab \leftarrow \{0\}^s$, $R \leftarrow \{0\}^{s \times s}$

$k \leftarrow k + 1$

22: **end while**

return x_k and estimated $(1 - \alpha)$ -interval

276876.

- [11] W. JOHNSON AND J. LINDENSTRAUSS, *Extensions of lipschitz maps into a hilbert space*, Contemporary Mathematics, 26 (1984), pp. 189–206, <https://doi.org/10.1090/comm/026/737400>.
- [12] E. KALNAY, *Atmospheric Modeling, Data Assimilation and Predictability*, Cambridge University Press, 2002, <https://doi.org/10.1017/CBO9780511802270>.
- [13] A. KRISHNAN, L. J. WILLIAMS, A. R. MCINTOSH, AND H. ABDI, *Partial least squares (pls) methods for neuroimaging: a tutorial and review*, Neuroimage, 56 (2011), pp. 455–475.
- [14] M. S. LAM, E. E. ROTHBERG, AND M. E. WOLF, *The cache performance and optimizations of blocked algorithms*, in ASPLOS IV, 1991.
- [15] J. MATOUŠEK, *On variants of the johnson–lindenstrauss lemma*, Random Structures & Algorithms, 33 (2008), pp. 142–156.
- [16] A. J. MILLER, *Algorithm as 274: Least squares routines to supplement those of gentleman*, Journal of the Royal Statistical Society. Series C (Applied Statistics), 41 (1992), pp. 458–478, <http://www.jstor.org/stable/2347583> (accessed 2022-04-29).
- [17] C. C. PAIGE AND M. A. SAUNDERS, *Lsqr: An algorithm for sparse linear equations and sparse least squares*, ACM Trans. Math. Softw., 8 (1982), p. 43–71, <https://doi.org/10.1145/355984.355989>, <https://doi.org/10.1145/355984.355989>.
- [18] V. PATEL, M. JAHANGOSHAHI, AND D. A. MALDONADO, *Convergence of adaptive, randomized, iterative linear solvers*, arXiv preprint arXiv:2104.04816, (2021).
- [19] V. PATEL, M. JAHANGOSHAHI, AND D. A. MALDONADO, *An implicit representation and iterative solution of randomly sketched linear systems*, SIAM Journal on Matrix Analysis and Applications, 42 (2021), pp. 800–831.
- [20] V. PATEL, M. JAHANGOSHAHI, AND D. A. MALDONADO, *Randomized block adaptive linear system solvers*, arXiv preprint arXiv:2204.01653, (2022).
- [21] M. PILANCI AND M. J. WAINWRIGHT, *Iterative hessian sketch: Fast and accurate solution approximation for constrained least-squares*, J. Mach. Learn. Res., 17 (2016), p. 1842 – 1879.
- [22] N. PRITCHARD AND V. PATEL, *Residual tracking and stopping for iterative random sketching*, 2022, <https://doi.org/10.48550/ARXIV.2201.05741>, <https://arxiv.org/abs/2201.05741>.
- [23] I. SELESNICK, *Least squares with examples in signal processing*, Connexions, 4 (2013).
- [24] K. SINGH, A. SANDU, M. JARDAK, K. W. BOWMAN, AND M. LEE, *A practical method to estimate information content in the context of 4d-var data assimilation*, SIAM/ASA Journal on Uncertainty Quantification, 1 (2013), pp. 106–138, <https://doi.org/10.1137/120884523>, <https://doi.org/10.1137/120884523>, <https://arxiv.org/abs/https://doi.org/10.1137/120884523>.
- [25] H. C. SO AND L. LIN, *Linear least squares approach for accurate received signal strength based source localization*, IEEE Transactions on signal processing, 59 (2011), pp. 4035–4040.
- [26] O. TALAGRAND AND P. COURTIER, *Variational assimilation of meteorological observations with the adjoint vorticity equation. i: Theory*, Quarterly Journal of the Royal Meteorological Society, 113 (1987), pp. 1311–1328.
- [27] A. TARAKANOV AND A. H. ELSHEIKH, *Regression-based sparse polynomial chaos for uncertainty quantification of subsurface flow models*, Journal of Computational Physics, 399 (2019), p. 108909, <https://doi.org/10.1016/j.jcp.2019.108909>, <https://doi.org/10.1016%2Fj.jcp.2019.108909>.
- [28] M. J. WAINWRIGHT, *High-Dimensional Statistics: A Non-Asymptotic Viewpoint*, Cambridge Series in Statistical and Probabilistic Mathematics, Cambridge University Press, 2019, <https://doi.org/10.1017/9781108627771>.
- [29] W. ZHANG AND N. HIGHAM, *Matrix depot: An extensible test matrix collection for julia*, PeerJ Computer Science, 2 (2016), p. e58, <https://doi.org/10.7717/peerj-cs.58>.